| 1 | Redefining Antibacterial Strategies with computational Screening of Benzimidazole Ligands |
|----------------|--|
| 2 | Against VanZ Protein for Alternatives of Antibiotic. |
| 3 | Vishma Pratap Sur ^{1*} , Madhab Kumar Sen ² , Aninda Mazumdar ³ . |
| 4 | |
| 5 6 | ¹ Laboratory of Reproductive Biology, Institute of Biotechnology of the Czech Academy of Sciences, BIOCEV, Prumyslova 595, 25250 Vestec, Czech Republic. |
| 7 8 9 | ² Department of Agroecology and Crop Production, Faculty of Agrobiology, Food and Natural Resources, Czech University of Life Sciences Prague, Kamýcká129, 165 00 Prague, Czech Republic. |
| 10 11 12 | ³ Laboratory for Biology of Secondary Metabolism, Institute of Microbiology of the Czech Academy of Sciences, Videnska 1083, 142 20 Prague Czech Republic. |
| L3 L4 | Vishma Pratap Sur* vishmapratapsur@gmail.com Author to whom correspondence should be addressed. |
| L5 | |
| L6 | |
| L7 | |
| L8 | |
| L9 | |
| 20 | |
| 21 | |
| 22 | |
| 23 24 | |
| 25 | |
| 26 | |
| 27 | |
| 28 | |
| 29 | |
| | |

Abstract

VanZ has crucial involvement in the modification of the bacterial peptidoglycan precursor and blocking its competence to bind with vancomycin and other related antibiotics. Hence targeting this protein can be an excellent option for combating the antibacterial resistance, particularly in the context of glycopeptide antibiotics like vancomycin. Hence, in this study, we have focused on the screening of 323 benzimidazole-based ligands for their possible interaction with the binding pocket of VanZ. The screening was based on the binding affinity values derived from molecular docking analysis. Furthermore, we had conducted an interacting amino acid analysis and we found six ligands that demand additional investigation. Consequently, we conducted molecular dynamics (MD) simulations using the optimal pose of VanZ to validate the stability of these VanZ–ligand complex and strengthen the consistency of the molecular docking results. Additionally, the pharmacological parameter was checked for all the six compounds. In summary, using the computational studies, we have successfully identified the putative candidates, which can be used for further in-vivo analyses. Our comprehensive approach can serve as a basis for the development of targeted compounds with enhanced efficacy against VanZ.

Key words: Antibacterial Resistance; Glycopeptide Antibiotics; Drug screening; Ligands;
 Molecular Docking; MD simulations.

Introduction

The emergence of antibiotic-resistant pathogenic bacteria has decreased the effectivity of novel antimicrobials and increased the need to develop a treatment against these pathogens as well as the existing antibiotics[1-3]. Various studies reporting antimicrobial resistance has been published by numerous scientists across the globe[1, 2, 4-7]. The evolution of vancomycin-resistant *S. aureus* (VRSA) and methicillin-resistant *S. aureus* (MRSA) has been reported by Bouche et al., 2010 [8] and Loomba et al., 2010[9]. These notable evidence of the development of resistant mechanism toward prominent broad-range antibiotics, has developed the urge to find alternatives to the conventional antibiotics[2, 8].

Reports from the United States [10] and Germany [11] showed that *E. faecium* is among the most common causes of healthcare-associated infections. The vanA gene cluster comprises of two additional genes: VanY and VanZ. VanY and VanZ provide high-level resistance to vancomycin and teicoplanin, respectively. VanY is known to hydrolyse the C-terminal D-Ala or D-Lac residue of peptidoglycan precursors but lacks transpeptidase activity [12-15]. Reports

shown that in media containing high concentrations of D-Ala, this enzyme promotes to 63 vancomycin resistance. Arthur et al., 1996 showed that VanY also contributes to resistance in 64 strains expressing vanH, vanA and vanX at a low level[16]. The mechanisms of VanZ-mediated 65 resistance have not been thoroughly explored yet in comparison to the other genes present in the 66 67 cluster. 68 The increase in the rates of microbial resistance, has triggered the attempts of researchers to identify and develop novel synthetic-compound based antimicrobial agents. Derivatives of 69 70 benzimidazole have shown promising capabilities to act as antimicrobial agents. Benzimidazole-71 containing compounds are known to have several antimicrobial properties such as antibacterial, antifungal and antiviral, besides having versatile bioactivities such as antitumor, antidepressant, 72 analgesic, anti-inflammatory and antidiabetic properties[17]. Benzimidazole-derivatives such as 73 thiabendazole, cambendazole, parbendazole, mebendazole are even known to have anti-helminth 74 properties, owing to which they are used to treat gastrointestinal worm infections in humans and 75 76 animals[18]. Additionally, earlier studies have also found that many benzimidazole-based 77 compounds can be effective in the treatment of Alzheimer's disease[2, 19]. The wide-ranging 78 interests in benzimidazole-containing compounds have promoted extensive studies with their structures. Previous studies from previous reports and our research works suggested that 79 80 benzimidazole based ligands showed promising antibacterial property [2, 5]. Hence, in this study, benzimidazole-based ligands were screened based on their binding affinity 81 values (obtained from molecular docking analysis) with the binding pocket of VanZ. An 82 interacting amino acid analysis was also performed to get additional information about the 83 participating amino acids in VanZ-ligands interaction. The best benzimidazole based candidates 84 were chosen based on the molecular docking scores. Thereafter, the molecular dynamics (MD) 85 simulation was performed with the best pose of VanZ to confirm the VanZ-ligand stability and 86 validate the molecular docking results [5, 20]. The results obtained from the combined docking and 87 88 simulation studies are expected to provide essential insights into the dynamic behavior and longterm stability of the identified ligands in the binding pocket of VanZ. 89

90

91

92

Results

2.1. Protein structure preparation and docking pocket analysis.

In this study, the 3D structure of VanZ was predicted as per our last work by using the I-TASSER web server to predict the 3D structure of VanZ (Figure 1A) [5]. Ten templates taken into consideration for the modelling had a Z-score >1 (TableS1). Five predicted models (Figure 1 and

S1) exhibited C-scores ranging from -2.01 to -4.7 (Table S1). The predicted structure of the VanZ had a high confident score for most of the amino acid sequence, see Figure S2. The predicted normalized B-factor value was mostly in the negative region of the axis (Figure S3). The overall results suggested that the model with the highest C-score (-2.01) Table S2 stands out as the most promising candidate for subsequent investigations and follow-up studies.

Before, performing molecular docking, docking pocket for ligand binding was analyzed by using CASTp. The structure was used to predict the binding pockets using CASTp. It was used to determine the binding pocket solvent accessible (SA) surface area and volume. The prediction analysis predicted at least six binding pockets distributed within both the interior and surface regions of the protein (Figure 2). For detailed information on the solvent volume (SA) and solvent area (SA) of these six binding pockets in VanZ can be found within the Table S3. It provides crucial insights into the spatial characteristics of these binding pockets, potential amino acids that can possess binding capacity against the benzimidazole ligands and emphasizes their significance as potential optimal sites for ligand binding Table S4.

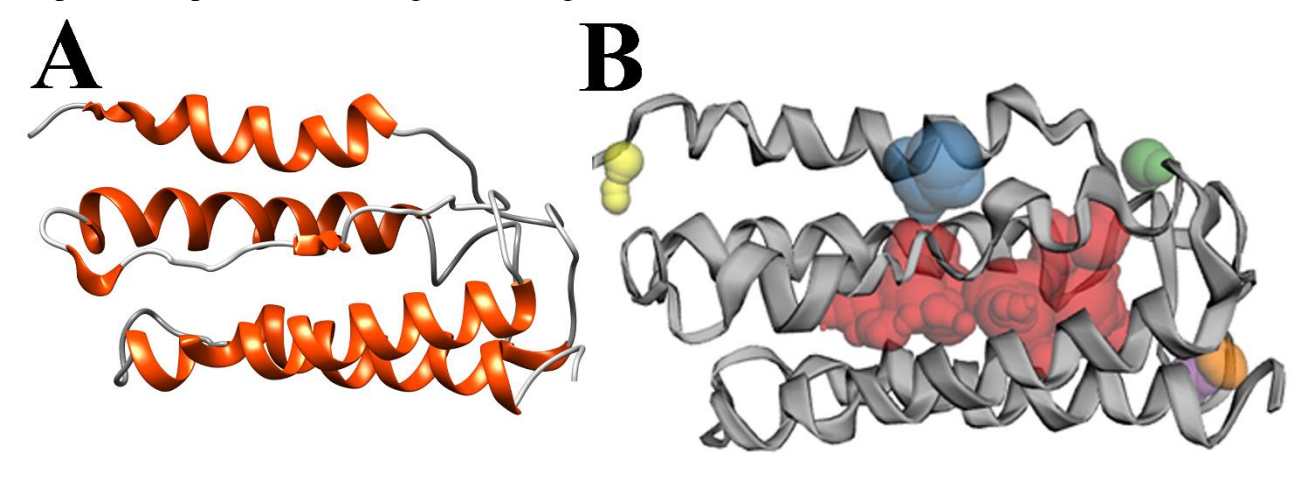


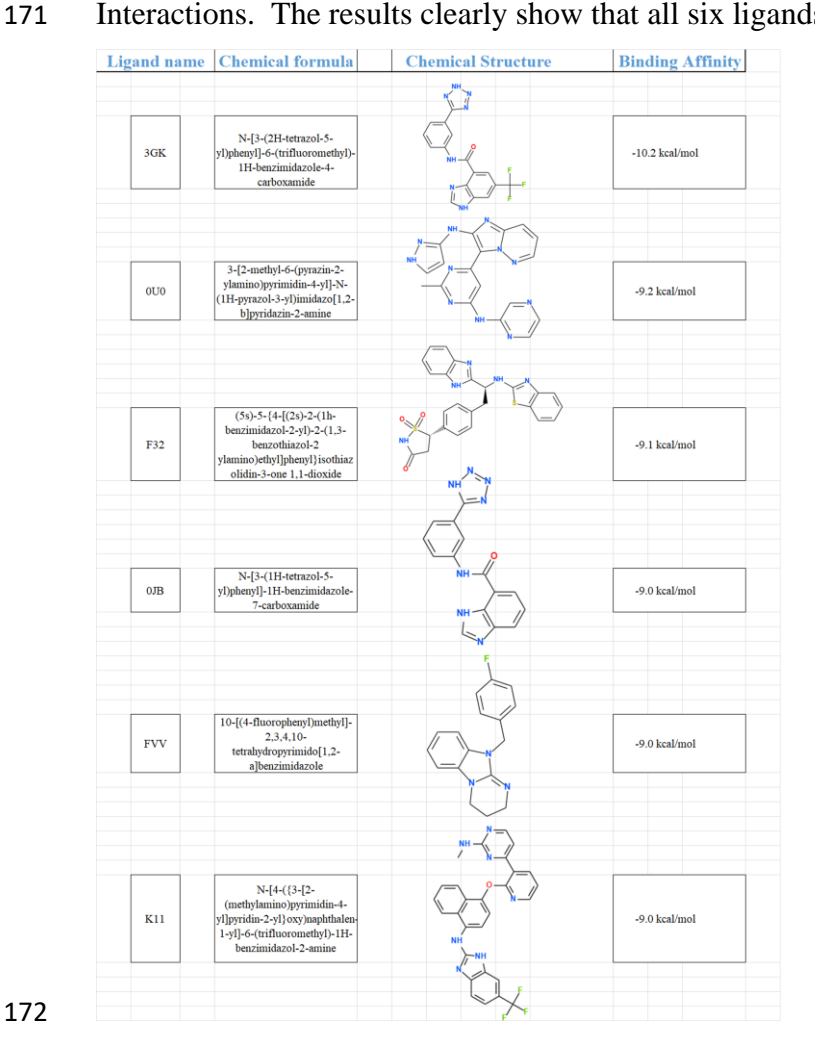
Figure 1: VanZ protein structural analysis. A. Schematic three-dimensional diagram of the VanZ protein showing the arrangements of various secondary structure. The structure was predicted by I-TASSER software using its default parameters. The software usually detects the structure of the templates based on fold recognition (or threading). B. Predicted ligand-binding pocket of the VanZ protein, using CASTp 3.0 software and its default parameters.

2.2. Ligand library preparation, Molecular Docking, and interaction analysis

To identify a potential VanZ inhibitors, structure-based molecular docking experiment was performed with 323 benzimidazole based compounds using target specific docking (pre-identified pocket with CastP). These selected compounds have therapeutic potential against cancer, infectious diseases, and some other diseases. Six compounds gave "best hit" docking score of

```
-10.2 to -9 kcal/mol (Figure 2 and Table 1). The list of compounds, based on their binding
122
           energies (PyRx based Vina scores) of the top hit ligands against VanZ, are shown in Table 1 and
123
          Figure 4. Six top hit ligand molecules were selected based on the top hit criteria and were further
124
          analyzed for molecular interactions with VanZ (Table 1, Figure 3, and Figure 4). The ligands are
125
           3GK (N-[3-(2H-tetrazol-5-yl)phenyl]-6-(trifluoromethyl)-1H-benzimidazole-4-carboxamide), 0U0
126
          (3-[2-methyl-6-(pyrazin-2-ylamino)pyrimidin-4-yl]-N-(1H-pyrazol-3-yl)imidazo[1,2-b]pyridazin-
127
          2-amine),
                                         F32
                                                               ((5s)-5-\{4-[(2s)-2-(1h-benzimidazol-2-yl)-2-(1,3-benzothiazol-2-yl)-2-(1,3-benzothiazol-2-yl)-2-(1,3-benzothiazol-2-yl)-2-(1,3-benzothiazol-2-yl)-2-(1,3-benzothiazol-2-yl)-2-(1,3-benzothiazol-2-yl)-2-(1,3-benzothiazol-2-yl)-2-(1,3-benzothiazol-2-yl)-2-(1,3-benzothiazol-2-yl)-2-(1,3-benzothiazol-2-yl)-2-(1,3-benzothiazol-2-yl)-2-(1,3-benzothiazol-2-yl)-2-(1,3-benzothiazol-2-yl)-2-(1,3-benzothiazol-2-yl)-2-(1,3-benzothiazol-2-yl)-2-(1,3-benzothiazol-2-yl)-2-(1,3-benzothiazol-2-yl)-2-(1,3-benzothiazol-2-yl)-2-(1,3-benzothiazol-2-yl)-2-(1,3-benzothiazol-2-yl)-2-(1,3-benzothiazol-2-yl)-2-(1,3-benzothiazol-2-yl)-2-(1,3-benzothiazol-2-yl)-2-(1,3-benzothiazol-2-yl)-2-(1,3-benzothiazol-2-yl)-2-(1,3-benzothiazol-2-yl)-2-(1,3-benzothiazol-2-yl)-2-(1,3-benzothiazol-2-yl)-2-(1,3-benzothiazol-2-yl)-2-(1,3-benzothiazol-2-yl)-2-(1,3-benzothiazol-2-yl)-2-(1,3-benzothiazol-2-yl)-2-(1,3-benzothiazol-2-yl)-2-(1,3-benzothiazol-2-yl)-2-(1,3-benzothiazol-2-yl)-2-(1,3-benzothiazol-2-yl)-2-(1,3-benzothiazol-2-yl)-2-(1,3-benzothiazol-2-yl)-2-(1,3-benzothiazol-2-yl)-2-(1,3-benzothiazol-2-yl)-2-(1,3-benzothiazol-2-yl)-2-(1,3-benzothiazol-2-yl)-2-(1,3-benzothiazol-2-yl)-2-(1,3-benzothiazol-2-yl)-2-(1,3-benzothiazol-2-yl)-2-(1,3-benzothiazol-2-yl)-2-(1,3-benzothiazol-2-yl)-2-(1,3-benzothiazol-2-yl)-2-(1,3-benzothiazol-2-yl)-2-(1,3-benzothiazol-2-yl)-2-(1,3-benzothiazol-2-yl)-2-(1,3-benzothiazol-2-yl)-2-(1,3-benzothiazol-2-yl)-2-(1,3-benzothiazol-2-yl)-2-(1,3-benzothiazol-2-yl)-2-(1,3-benzothiazol-2-yl)-2-(1,3-benzothiazol-2-yl)-2-(1,3-benzothiazol-2-yl)-2-(1,3-benzothiazol-2-yl)-2-(1,3-benzothiazol-2-yl)-2-(1,3-benzothiazol-2-yl)-2-(1,3-benzothiazol-2-yl)-2-(1,3-benzothiazol-2-yl)-2-(1,3-benzothiazol-2-yl)-2-(1,3-benzothiazol-2-yl)-2-(1,3-benzothiazol-2-yl)-2-(1,3-benzothiazol-2-yl)-2-(1,3-benzothiazol-2-yl)-2-(1,3-benzothiazol-2-yl)-2-(1,3-benzothiazol-2-yl)-2-(1,3-benzothiazol-2-yl)-2-(1,3-benzothiazol-2-yl)-2-(1,3-benzothiazol-2-yl)-2-(1,3-benzothiazol-2-yl)-2-(1,3-benzothiazol-2-yl)-2-(1,3-benzothiazol-2-yl)-2-(1,3-benzothiazol-2-yl)-
128
          ylamino)ethyl]phenyl}isothiazolidin-3-one 1,1-dioxide), 0JB (N-[3-(1H-tetrazol-5-yl)phenyl]-1H-
129
                                                                            FVV
130
          benzimidazole-7-carboxamide),
                                                                                                      (10-[(4-fluorophenyl)methyl]-2,3,4,10-
          tetrahydropyrimido[1,2-a]benzimidazole),
131
                                                                                   K11
                                                                                                   (N-[4-({3-[2-(methylamino)pyrimidin-4-
          yl]pyridin-2-yl}oxy)naphthalen-1-yl]-6-(trifluoromethyl)-1H-benzimidazol-2-amine). 3GK [21]
132
          showed the highest binding energy, -10.2 kcal/mol, with the VanZ. The results showed two
133
          hydrogen bonds with two VanZ residues, Asn111, Ser88 (Table 1). 3GK also showed 5 different
134
          interactions (Halogen, Pi-Sigma, Pi-Pi T-Shaped, Alkyl and Pi-alkyl) with 8 different residues,
135
           Val84, Gly118, Leu148, Tyr152, Ile93, Ile60, Val141, Leu145, of the VanZ protein (Figure 3A-3B
136
          and Table 1).
137
          In terms of top hit ligands depending on the highest binding energy, the other five potent
138
139
          benzimidazole based compounds were 0U0, F32, 0JB, FVV, K11 (Table1, Figure 3 and Figure 4).
          0U0 (an investigational molecules against cancerous growth factor) [22] showed -9.2 kcal/mol
140
          binding energy against VanZ (Table 1 Figure 3C-3D). The molecular level interaction prediction
141
          study showed two hydrogen bonds with VanZ residues, Ile59, Val84. 0U0 also showed 1 group of
142
          electrostatic and 2 group of hydrophobic interactions (Pi-Sigma, Alkyl and Pi Alkyl) with 7
143
          different residues Val141, Ile60, Leu145, Leu148, Ile138, Val86, Ile93 (Table 1 Figure 3C-3D).
144
          F32 (an investigational drug against diabetes type II) [23] showed -9.1 kcal/mol binding energy
145
          against VanZ (Table 1 Figure 3E-3F). The interaction study showed four hydrogen bonds with
146
           VanZ residues, two with Thr46, one with Asn41 and another with Tyr152, while F32 showed
147
          electrostatic interaction (Pi Sigma) with two VanZ residues named Thr48, Val151, and
148
          hydrophobic interactions (Pi-Alkyl) with 4 VanZ residues namedArg52, Leu144, Val147, (Table 1
149
          Figure 3E-3F). 0JB (an investigational β-Lactamase inhibitory molecule) [24] showed –9 kcal/mol
150
          binding energy against VanZ protein (Table 1 Figure 4A-4B). The interaction prediction study
151
          showed two hydrogen bonds with two VanZ residues, Arg52 and Ser88, also on 0JB, showed six
152
          mixed interactions (Carbon Hydrogen Bond, Unfavorable Donor-Donor, Pi-Cation, Pi-Sigma, Pi-
153
          Pi-T-Shaped, Pi-Alkyl) with 8 VanZ residues Asp56, Arg52, Leu148, Tyr152, Ile60, Ile93,
154
          Val141, Leu145 (Table 1 Figure 4A-4B). FVV (an investigational anti-cancer drug) [25] showed
155
```

-9 kcal/mol binding energy against VanZ protein (Table 1 Table 1 Figure 4C-4D). The interaction prediction study showed no hydrogen bonds with VanZ residues, but FVV, showed three mixed interactions named alternative hydrogen bonding, electrostatic interactions, and hydrophobic interactions (Carbon Hydrogen Bond, Pi-Sigma, Alkyl and Pi-Alkyl) with 7 VanZ residues Lys80, Val141, Val84, Ile60, Ile138, Leu144, Leu145 (Table 1 Figure 4A-4B). K11 (an investigational angiogenesis drug) [26] also showed -9 kcal/mol binding energy against VanZ protein (Table 1 Figure 4E-4F). The interaction prediction study showed one hydrogen bonds with VanZ residue Glu92, also FVV, showed five mixed interactions (Carbon Hydrogen Bond, Halogen, Unfavorable Donor-Donor, Pi-Sigma, Alkyl and Pi-Alkyl) with 8 VanZ residues Gln95, Gly8, Ala11, Val15, Ile18, Phe64, Leu85, Leu87 (Table 1 Figure 4E-4F). Our molecular docking and interaction analysis study clearly indicates that these six investigational ligands showed very promising higher interaction with VanZ in terms of energy and residues involved in protein-ligand interactions. A molecular interaction study reveals that all top hit six ligands formed a smaller number of hydrogen bonds, whereas all ligands exert higher number of hydrophobic and electrostatic forces which indicates very strong protein-ligand Interactions. The results clearly show that all six ligands have highest possibility of bindings.



156

157

158

159

160

161

162

163

164

165

166

167

168

169

Figure 2: List of screened benzimidazole-based ligands with their chemical formulas and binding affinity scores against VanZ protein. The chemical formulas and their structures were retrieved from PubChem (https://pubchem.ncbi.nlm.nih.gov/).

Table 1: Benzimidazole Ligands binding affinity and hydrogen bond interactions against VanZ protein.

| Ligand | Binding Affinity (kcal/mol) | No. of H- bonds | H-bonds and interacting residues | Binding Affinity (kcal/mol | No. of other intera ctions | Other interactions and numbers | Other interaction and interacting residues |
|------------|-----------------------------------|-----------------------|---|----------------------------------|----------------------------|--|---|
| 3GK | -10.2 | 3 | Asn111 (2), Ser88 (1) | -10.2 | 12 | Halogen (4), Pi-Sigma (1), Pi-Pi T-Shaped (1), Alkyl and Pi-alkyl (6) | Val84 (2), Gly118 (2), Leu148 (2), Tyr152 (1), Ile93 (1), Val141 (2), Leu145 (2) |
| 0U0 | -9.2 | 4 | Ile59 (1), Val84 (1), Ser88 (2) | -9.2 | 10 | Pi-Sigma (6), Alkyl and Pi Alkyl (4) | Ile60 (1), Val84 (1), Val141(2), Leu145(2), Leu148(1), Val86(1), Ile93(1), Ile138(1) |
| F32 | -9.1 | 4 | Asn41(1), Thr46(2), Tyr152(1) | -9.1 | 6 | Pi-Sigma (2), Pi-Alkyl (4) | Thr48(1), Val151(1), Arg52(1), Leu144(1), Val147(1), Leu148(1) |
| 0JB | -9 | 2 | Arg52(1), Ser88(1) | -9 | 9 | Carbon Hydrogen Bond (1), Unfavorable Donor-Donor (1), Pi-Cation (1), Pi-Sigma (1), Pi-Pi-T- Shaped (1), Pi- Alkyl (4) | Arg52(2), Leu148(2), Tyr152(1), Ile93(2), Val141(1), Leu145(1) |
| FVV | -9 | - | - | -9 | 8 | Carbon Hydrogen Bond (2), Pi- Sigma (2), Alkyl and Pi- Alkyl (4) | Lys80(1), Val141(3), Val84(1), Ile60(1), Ile138(1), Leu145(1) |

| K11 | -9 | 3 | Glu92(2), | -9 | 11 | Carbon | Gln95(2), |
|-----|----|---|------------------|----|----|----------------|-------------------|
| | | | Val15 (1) | | | Hydrogen | Gly8 (1), |
| | | | | | | Bond (1), | Ala11 (3), |
| | | | | | | Halogen (1), | Val15(4), |
| | | | | | | Unfavorable | Ile18 (1), |
| | | | | | | Donor-Donor | Phe64 (1) |
| | | | | | | (1), Pi-Sigma | |
| | | | | | | (3), Alkyl and | |
| | | | | | | Pi-Alkyl (9) | |



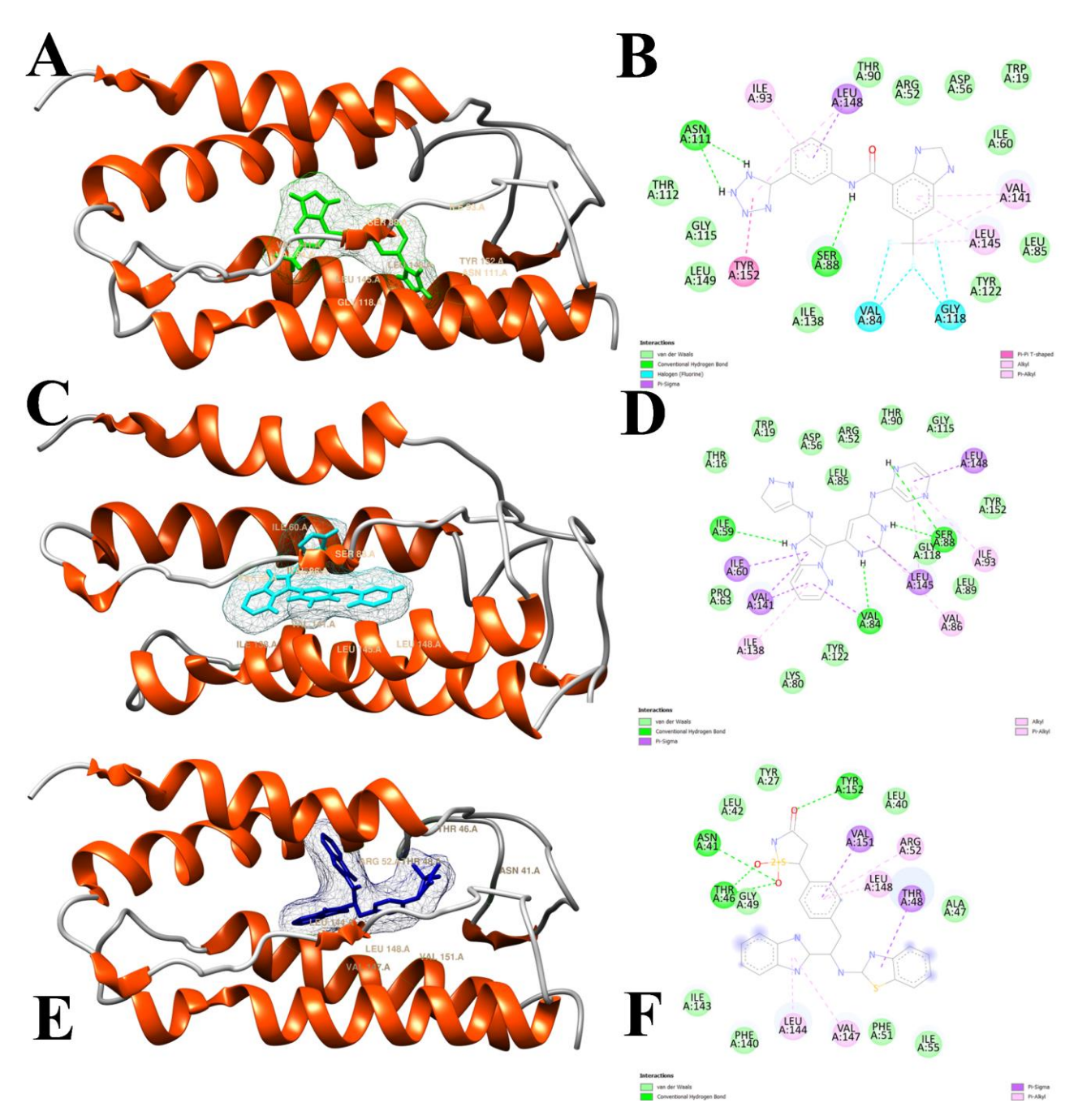


Figure 3. Molecular interactions and binding poses of the VanZ Protein with three benzimidazole ligands. (A & B) The binding poses and interacting residues of 3GK with VanZ. The binding affinity value was predicted as -10.2 kcal/mol and the interacting bonds ranged from van der

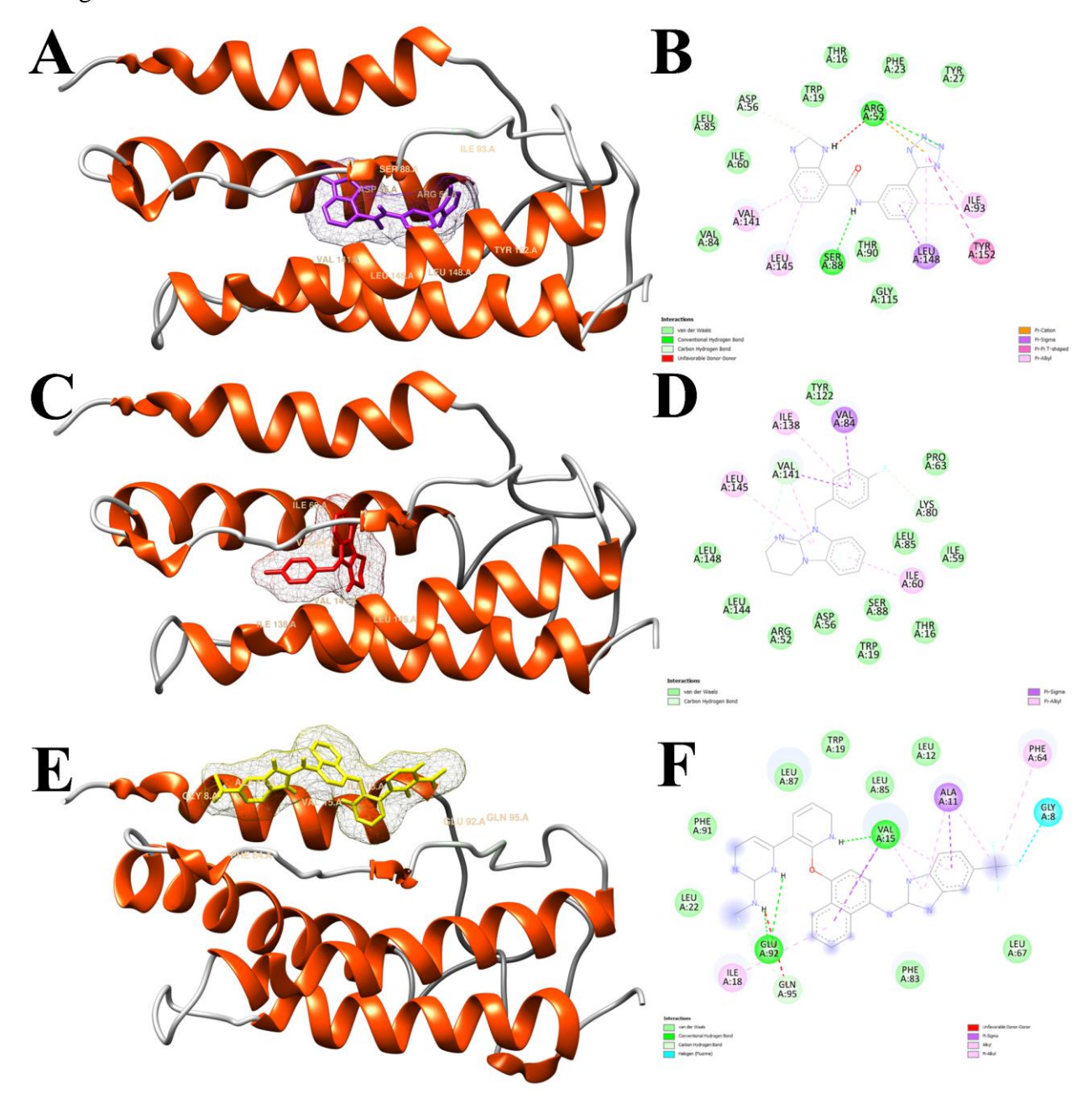


Figure 4: Molecular interactions and binding poses of the VanZ Protein with the other three benzimidazole ligands. (**A & B**) The binding poses and interacting residues of 0JB with VanZ. The interacting bonds ranged from van der Waals forces to Pi-Alkyl bonds. 17 interacting amino acids were predicted; (**C & D**) The binding poses and interacting residues of FVV with VanZ. 17 interacting amino acids were predicted. The interacting bonds were van der Waals forces, convectional H-bonds, Pi-Alkyl and Pi-Sigma bonds; (**E& F**) The binding pose and interacting

residues of K11, with VanZ. The predicted interacting bonds ranged from van der Waals forces to

198 Pi-Alkyl bonds. In all the cases the binding affinity value was predicted as -9 kcal/mol.

2.3. Crosschecking docking and interaction of the top hit ligands

199

To cross check the pyrx autodock vina docking results Swissdock server and Medusa server was 200 used for further docking the top hit six ligands, analysis their docking scores and later discovery 201 202 studio biovia visualizer was used for interacting amino acids identification. Swiss dock study indicates that 3GK (Figure 5A) showed the highest binding energy, -10.33 kcal/mol, with the 203 VanZ (Table 2 and Figure 5A-5B). The results showed no hydrogen bonds but 3GK showed 13 204 different interactions (Carbon Hydrogen Bond, Unfavorable Donor-Donor, Pi-Cation, Alkyl or Pi-205 Alkyl, Halogen, Metal Acceptor) with 10 different residues, Arg52, Trp19, Val84, Leu85, Ile93, 206 Ser88, Ile138, Val141, Leu145, Leu148, of the VanZ protein (Table 2 and Figure 5A-5B). In terms of 207 top hit ligands depending on the highest binding energy, the other five potent benzimidazole based 208 compounds were 0U0 (-9.36 kcal /mol), F32 (-10.2 kcal/mol), 0JB (-9.44 kcal/mol), FVV (-9.22 209 kcal/mol), K11 (-9.18 kcal/mol) (Table2, Figure 5 and Figure 6). 0U0 (Table 2 and Figure 5C-5D) 210 211 showed -9.36 kcal/mol binding energy against VanZ (Table 2 and Figure 5C-5D). The molecular level interaction prediction study showed no hydrogen bonds with VanZ residue. 0U0 also showed 212 2groups of Pi-cation 1 Pi-Pi T-shaped and 8 Alkyl and Pi-Alkyl (hydrophobic interactions) with 9 213 214 different residues Thr48, Leu40, Arg52, Leu144, Val147, Leu148, Leu150, Val151, Val152 (Table 2 and Figure 5C-5D).F32 showed -10.05 kcal/mol binding energy and binding pattern with 215 216 VanZ (Table 2 and Figure 5E-5F). The interaction study showed two hydrogen bonds with VanZ residue, with Asn41, while F32 showed electrostatic interaction (Pi cation) with one VanZ 217 residues named Leu148, one Pi- sulfur interactions with Tyr27 residue, and hydrophobic interactions 218 (Pi-Alkyl) with 3 VanZ residues named Leu40, Arg52, Val151 (Table 2 and Figure 5E-5F).0JB 219 220 showed –9.44 kcal/mol binding energy and binding pattern with VanZ protein (Figure 6A and Table 2). The interaction prediction study showed no hydrogen bonds with VanZ residues, also on 0JB, 221 showed 9 mixed interactions Alkyl and Pi-Alkyl and Unfavorable bump with 6 VanZ residues 222 Asp56, Ile93, Val141, Leu144, Leu145, Leu148(Table 2 and Figure 6A-6B).FVV showed -9.22 223 kcal/mol binding pattern with residues and the energy with VanZ protein (Table 2 and Figure 6C-224 6D). The interaction prediction study showed one hydrogen bonds with Ser88 VanZ residue, FVV 225 also showed 10 mixed interactions named alternative hydrogen bonding, electrostatic interactions, 226 and hydrophobic interactions (Carbon Hydrogen Bond, Pi-cation, Alkyl and Pi-Alkyl, Metal 227 Acceptor) with 9 VanZ residues Ile60, Val84, Leu85, Ser88, Tyr122, Ile138, Val141, Leu145, 228 (Table 2 and Figure 6C-6D).K11 also showed -9.18 kcal/mol binding energy and binding pattern 229 with interacting residues with VanZ protein (Table 2 and Figure 6C-6D). The interaction prediction 230

study showed no hydrogen bonds with VanZ residue. K11 showed 12 mixed interactions (Metal Acceptor, Halogen, Pi-Pi-T-shaped, Alkyl and Pi-Alkyl and covalent bond) with 7 VanZ residues Ala11, Val15, Pro79, Phe72, Phe83, Leu87, Leu85(Table 2 and Figure 6C-6D).

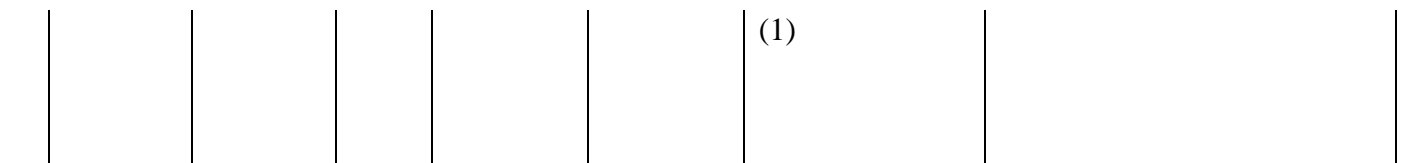
231

232

233

Table 2: Benzimidazole Ligands binding affinity and hydrogen bond interactions against VanZ protein, though swissdock re-docking.

| Ligands | Binding Affinity (kcal/m ol) | No. of H- bon ds | H-bonds and interacti ng residues | No. of other interactions | Other interactions and numbers | Other interaction and interacting residues |
|---------|---------------------------------------|------------------------------|---|---------------------------|--|--|
| 3GK | -10.33 | 0 | | 13 | Carbon Hydrogen Bond (2), Unfavorable Donor-Donor (1), Pi-Cation (1), Alkyl or Pi-Alkyl (7), Halogen (1), Metal Acceptor (1) | Arg52 (2), Trp19 (1), Val84 (1), Leu85 (1), Ile93 (1), Ser88 (1), Ile138 (1), Val141 (1), Leu145 (2), Leu148 (2) |
| 0U0 | -9.36 | 0 | | 11 | Pi-cation (2), Pi-Pi T-shaped (1) Alkyl and Pi-Alkyl (8) | Thr48 (1), Leu40 (2), Arg52 (1), Leu144 (1), Val147 (1), Leu148 (1), Leu150 (1), Val151 (2) Val152 (1) |
| F32 | -10.2 | 2 | Asn41 (2) | 6 | Pi-Cation (1), Pi-Alkyl (4), Pi sulfur (1) | Tyr27 (1), Leu40 (1), Arg52 (2), Leu148 (1), Val151 (1) |
| ОЈВ | -9.44 | 0 | | 9 | Alkyl and Pi- Alkyl (8), Unfavorable bump (1) | Asp56 (1), Ile93 (1), Val141 (2), Leu144 (1), Leu145 (2), Leu148 (2), |
| FVV | -9.22 | 1 | Ser88 | 10 | Carbon Hydrogen Bond (2), Pi-cation (2), Alkyl and Pi-Alkyl (4), Metal Acceptor (2) | Ile60 (1), Val84 (1), Leu85 (1), Ser88 (2), Tyr122 (1), Ile138 (1), Val141 (1), Leu145 (1), Leu148 (1) |
| K11 | -9.18 | | | 12 | Metal Acceptor (1), Halogen (2), Pi-Pi-T- shaped (1), Alkyl and Pi- Alkyl (7), Covalent bond | Ala11 (1), Val15 (2), Pro79 (1), Phe72 (3), Phe83 (3), Leu87 (1), Leu85 (1) |





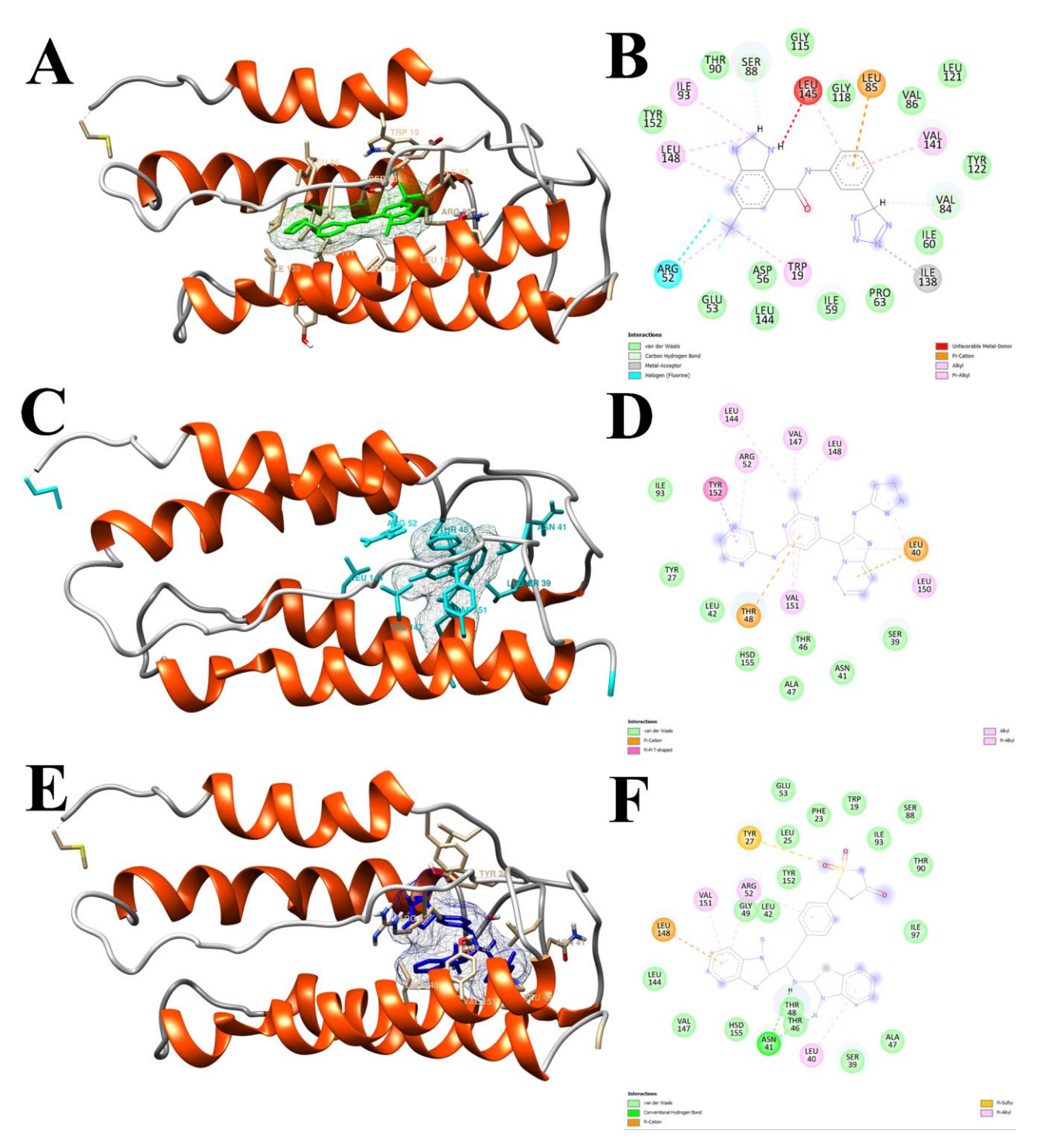


Figure 5: Crosschecking docking and molecular interactions of **(A)** 3GK, **(C)** 0U0 and **(E)** F32 with VanZ protein. Swiss dock server was used to cross-validate the molecular docking results predicted by AutoDock Vina. Figure 5B, 5D and 5F represents the interacting amino acids of the 3GK, 0U0 and F32 with VanZ protein, respectively.

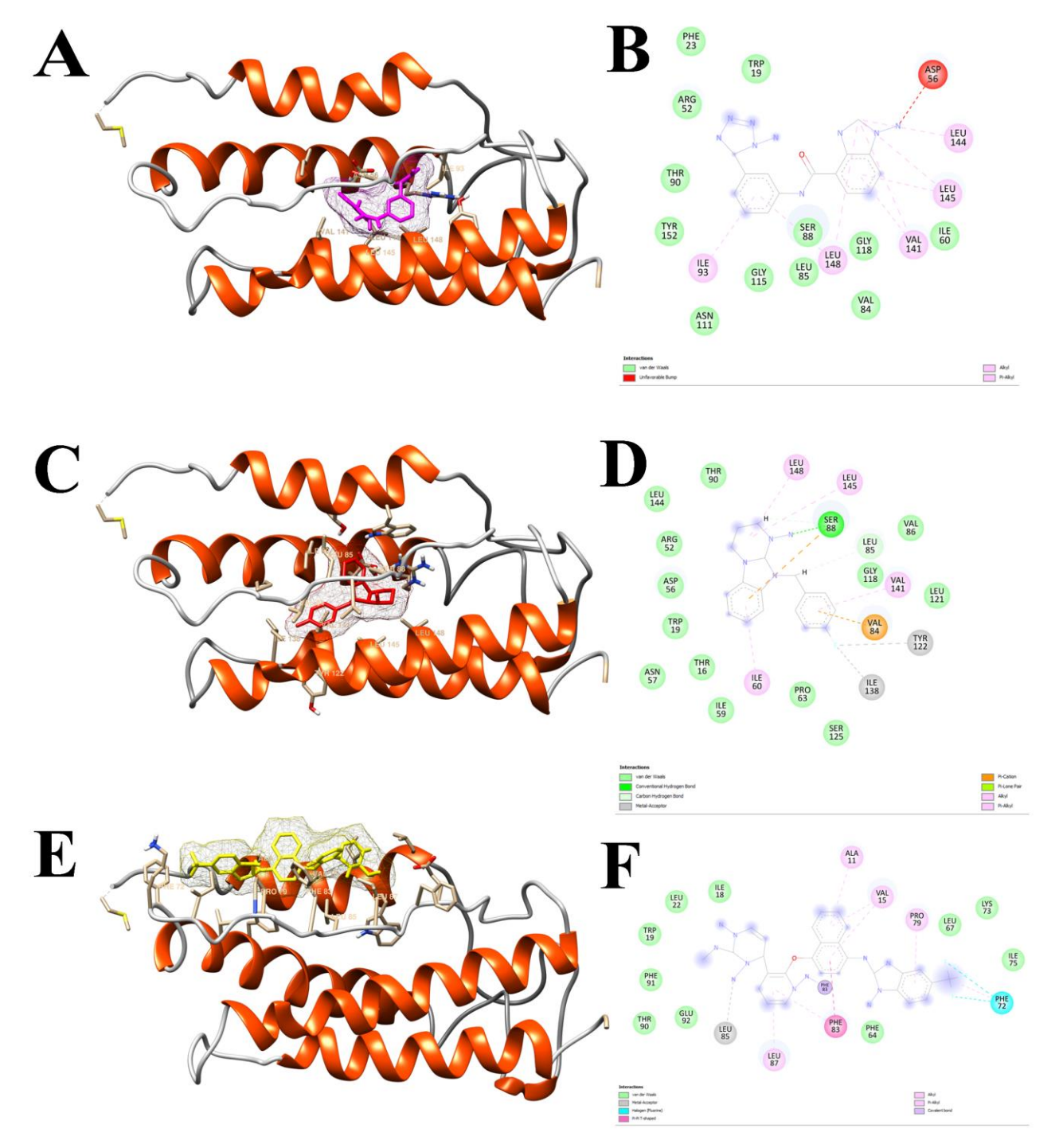


Figure 6: Crosschecking docking and molecular interactions of **(A)** 0JB, **(C)** FVB and **(E)** K11 with VanZ protein. Swiss dock server was used to cross-validate the molecular docking results predicted by AutoDock Vina. Figure 6B, 6D and 6F represents the interacting amino acids for the interaction between VanZ and the benzimidazole ligands (0JB, FVB and K11, respectively).

Medusa docking server support and agreeing our PyRx based docking and Swissdocking results where 3GK (Table 3 and Figure 7A-7B) showed the highest binding energy, -42.95 kcal/mol, with the VanZ (Table 3). The results showed two hydrogen bonds with two VanZ residues named Ser88,

```
Tyr152. 3GK showed 15 different interactions (Carbon Hydrogen Bond, Pi-Cation, Alkyl or Pi-
251
      Alkyl, Halogen, Pi-Sigma) with 11 different residues, Thr16, Trp19, Arg52, Asp56, Ile60, Val84,
252
      Val85, Ile93, Leu141, Leu145, Leu148, of the VanZ protein (Table 3 and Figure 7A-7B).
253
      In terms of top hit ligands depending on the highest binding energy, the other five potent
254
      benzimidazole based compounds were 0U0 (-38.69 kcal /mol), F32 (-46.92 kcal/mol), 0JB (-36.49
255
      kcal/mol), FVV (-34.42 kcal/mol), K11 (-30.35 kcal/mol). 0U0 showed -38.69 kcal/mol binding
256
      energy against VanZ (Table 3 and Figure 7C-7D). The molecular level interaction study of 0U0
257
      showed three hydrogen bonds with VanZ residue Tyr27, Asp56, Ser88. 0U0 also showed 1 group of
258
259
      Carbon Hydrogen Bond, 2 Pi-cation and 7 group of hydrophobic interactions (Alkyl and Pi Alkyl)
      with 8 different residues Arg52, Aap56, Leu145, Leu148, Ile93, Leu144, Val141, Asn111 (Table 3
260
      and Figure 7C-7D). F32 showed -46.92 kcal/mol binding energy and pattern with the residues
261
      against VanZ (Table 3 and Figure 7E-7F). The interaction study showed three hydrogen bonds with
262
      VanZ residue, with Asp56, Ile59, Lys80, while F32 showed interactions with five Pi-Sigma, five Pi-
263
      Alkyl, one Carbon Hydrogen Bond, three Pi-anion, one Unfavorable Positive-Positive VanZ residues
264
      named Arg52, Asp56, Ile60, Lys80, Ile93, Val141, Leu145, Leu144, Leu148 (Table 3 and Figure
265
      7E-7F).0JB showed -36.49 kcal/mol binding energy and binding pattern with the residues against
266
      VanZ protein (Table 3 and Figure 8A-8B). The interaction prediction study showed three hydrogen
267
268
      bonds with three VanZ residues, Arg52, Val84, Ser88, also on 0JB, showed ten mixed interactions
      Pi-Cation, Pi-Sigma, Alkyl/Pi-Alkyl with 7 VanZ residues Arg52, Ile60, Val86, Val141, Leu144,
269
      Leu145, Leu148(Table 3 and Figure 8A-8B).
270
      FVV showed -34.42 kcal/mol binding energy and binding pattern with interacting residues against
271
      VanZ protein (Table 3 and Figure 8C-8D). The interaction prediction study showed two hydrogen
272
      bonds with Arg52, Ser88 VanZ residue, FVV also showed 14 mixed interactions named alternative
273
274
      hydrogen bonding, electrostatic interactions, and hydrophobic interactions (Carbon Hydrogen Bond,
      Pi-sigma, Pi-Pi-T-shaped, Pi-anion and Alkyl and Pi-Alkyl) with nine VanZ residues Trp19, Leu85,
275
      Ile93, Asp56, Ser88, Val141, Leu144, Leu145, Leu148 (Table 3 and Figure 8C-8D).K11 also
276
      showed -30.35 kcal/mol binding energy and binding pattern with the interacting residues against
277
      VanZ protein (Table 3 and Figure 8E-8F). The interaction prediction study showed two hydrogen
278
      bonds with VanZ residue Asp56, Ser88, also FVV, showed fifteen mixed interactions (Metal
279
      Acceptor, Alkyl and Pi-Alkyl) with 10 VanZ residues Asn41, Ile60, Ile59, Pro63, Lys80, Val84,
280
      Ile93, Val141, Leu145, Leu148 (Table 3 and Figure 8E-8F).
281
282
```

| Ligand | Binding Affinity (kcal/mol) | No. of other interactions | No. of H-bonds | H-bonds and interacting residues | Other interactions and numbers | Other interaction and interacting residues |
|--------|-----------------------------------|---------------------------|-------------------|---|---|---|
| 3GK | -42.95 | 15 | 2 | Ser88 (1), Tyr152 (1) | Halogen (3), Pi-Sigma (2), Pi- cation/anion (2), Alkyl and Pi-alkyl (7), Carbon Hydrogen Bond (1) | Val84 (2), Leu85 (1), Arg52 (1), Asp56 (1), Trp19 (1), Ile60 (1), Leu148 (1), Ile93 (2) Val141 (2), Leu145 (2), Thr16 (1). |
| ouo | -38.69 | 12 | 3 | Tyr27 (1), Asp56 (1), Ser88 (1) | Pi-Sigma (2), Alkyl and Pi Alkyl (7), Pi- cation/anion (2), Carbon Hydrogen Bond (1) | Arg52 (3), Aap56 (1), Leu145 (2), Leu148 (2), Ile93 (1), Leu144 (1), Val141 (1), Asn111 (1) |
| F32 | -46.92 | 15 | 3 | Asp56 (1), Ile59 (1), Lys80 (1) | Pi-Sigma (5), Pi-Alkyl (5), Carbon Hydrogen Bond (1), Pi- anion (3), Unfavorable Positive- Positive (1) | Arg52 (1), Asp56 (3), Ile60 (1), Lys80 (1), Ile93 (1), Val141 (1), Leu145 (1), Leu144 (1), Leu148 (4) |
| ОЈВ | -36.49 | 10 | 3 | Arg52 (1), Val84 (1), Ser88 (1) | Pi-Cation (1), Pi-Sigma (1), Alkyl/Pi- Alkyl (8) | Arg52 (1), Ile60 (1), Val86 (1), Val141 (2), Leu144 (1), Leu145 (3), Leu148 (1) |
| FVV | -34.42 | 14 | 2 | Arg52 (1), Ser88 (1) | Carbon Hydrogen Bond (2), Pi-Sigma (1), Pi-Pi-T- shaped (1), Pi-Anion (2), Alkyl and Pi- | Trp19 (1), Leu85 (1), Ile93 (1), Asp56 (2), Ser88 (1), Val141 (1), Leu144 (1), Leu145 (3), Leu148 (3) |

| | | | | | Alkyl (8) | |
|-----|--------|----|---|-----------------|-------------------------------|--|
| K11 | -30.35 | 15 | 2 | Asp56, Ser88 | Halogen (2), Pi-Sigma (4), | Asn41 (1), Ile60 (2), Ile59 (1), Pro63 (1), Lys80 (1), Val84 (1), Ile93 (1),Val141 (3), Leu145 (2), Leu148 (2) |



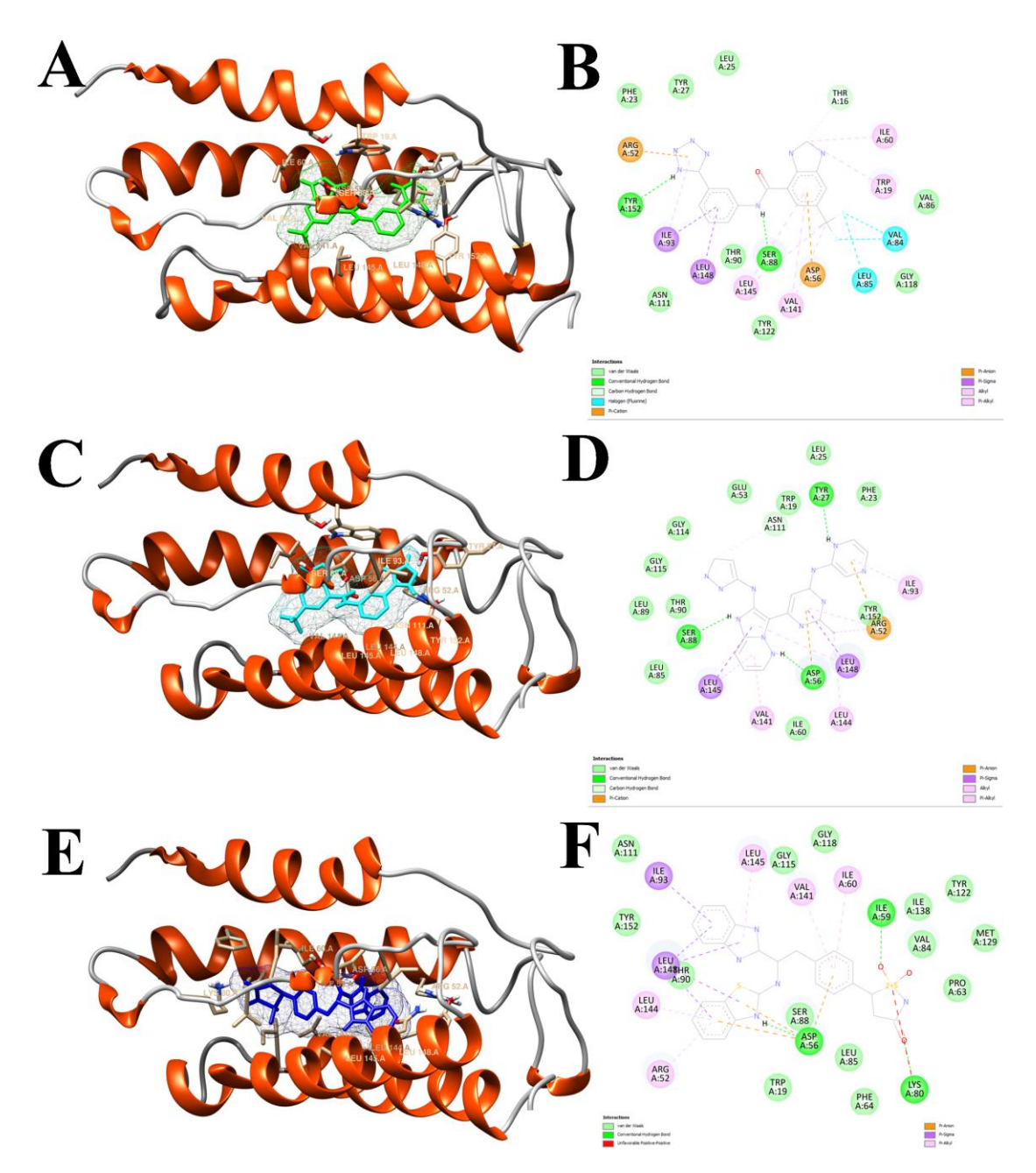


Figure 7: Crosschecking docking and molecular interactions of **(A)** 3GK, **(C)** 0U0 and **(E)** F32 with VanZ protein using Medusa Dock software. Figure 7B, 7D and 7F represents the interacting amino acids of the 3GK, 0U0 and F32 with VanZ protein, respectively.

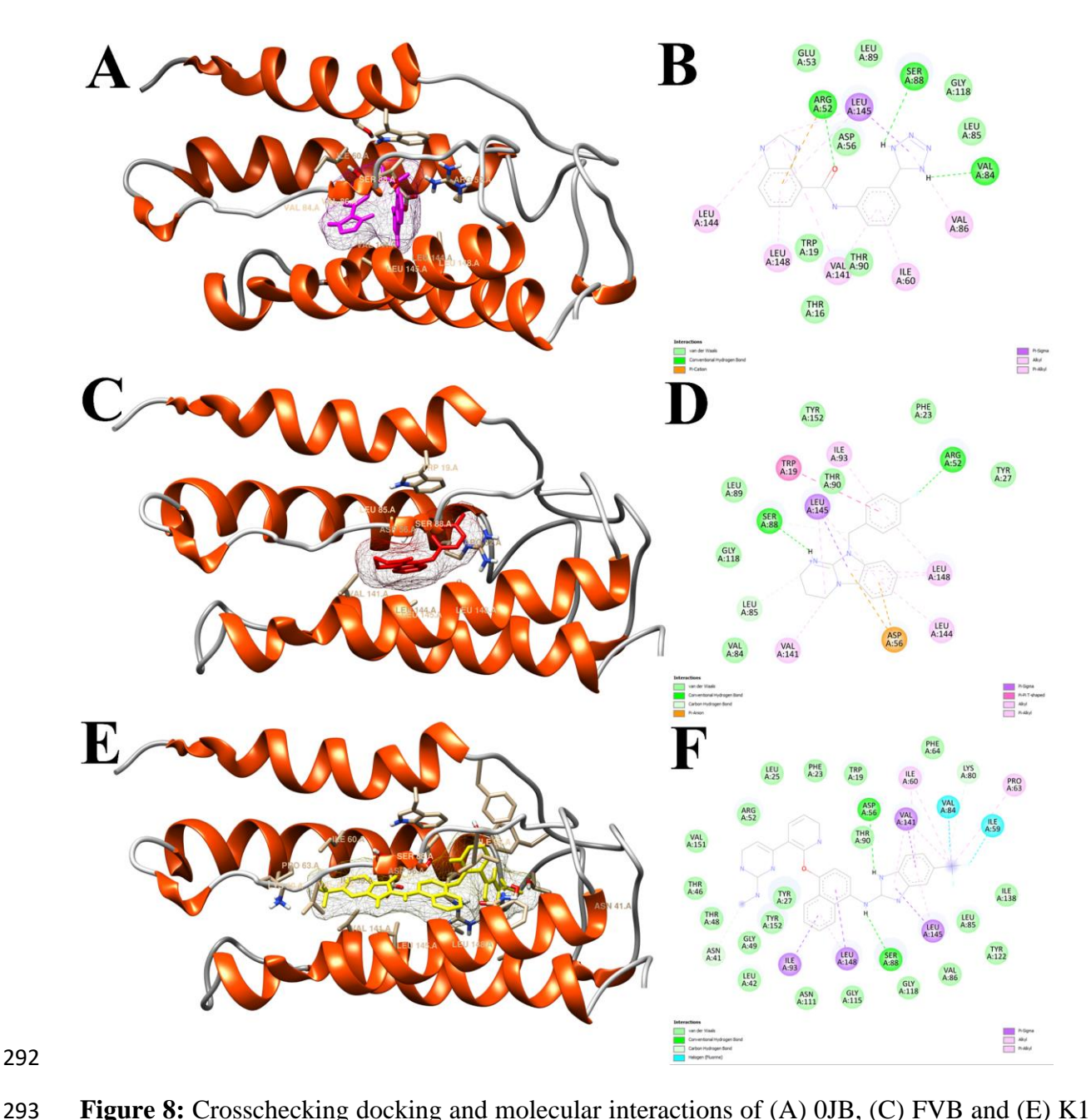


Figure 8: Crosschecking docking and molecular interactions of (A) 0JB, (C) FVB and (E) K11 with VanZ protein. Medusa Dock software was used to cross-validate the molecular docking results predicted by AutoDock Vina. Figure 8B, 8D and 8F represents the interacting amino acids for the interaction between VanZ and the benzimidazole ligands (0JB, FVB and K11, respectively).

Our molecular re-docking investigation conducted using both Swiss dock and Medusa dock servers distinctly demonstrates that the six investigational drug ligands exhibit remarkably high interaction energy. This energy profile aligns closely with the PyRx docking scores, underscoring the precision of our findings regarding the binding pocket, binding pose, and interaction energy. Notably, the molecular interaction study reveals a minimal presence of hydrogen bonds in all top six ligands. Instead, these ligands manifest a substantial prevalence of hydrophobic and electrostatic forces,

indicating robust protein-ligand interactions, a phenomenon consistent with our earlier observations

304 using Autodock Vina and PyRx docking.

Moreover, our re-docking analyses, executed through three distinct processes, consistently highlight

similar interacting amino acids across all ligands when targeting the VanZ protein. This robust

307 concurrence further reinforces the validity of our predictions and analyses.

308 Both of our docking study mostly agreeing in terms of binding energy and interactive amino acids

(Table 1, Table 2 and Table 3). According to our knowledge there are no such inhibitors against

VanZ protein with such high binding affinities, but our results clearly showing that all six ligands

have highest possibility of bindings. Out of six ligands four (3GK, F32, 0JB, FVV) showed similar

interactive amino acids which clearly indicates the docking accuracy and confirmed interacting

amino acids of VanZ with benzimidazole based drugs. Here we are proposing six possible ligands

against VanZ with promising protein-drug interactions.

315

323

325

326

327

328

329

330

331

306

309

311

312

313

314

316 2.4. Absorption, Distribution, Metabolism, Excretion, and Toxicity (ADMET) Analysis

317 2.4.1. Absorption

318 Drug absorption is mainly analyzed through the water solubility of ligands, cell permeability using

319 colon carcinoma (Caco-2) cell line, human intestinal absorption, skin permeability, and whether the

molecule is a P-glycoprotein substrate or inhibitor [27]. The ligand's water solubility reflects the

321 ligands water solubility at 25 °C. All the selected six ligands are moderately soluble in water (Table

3). Caco-2 cell permeability and human intestinal absorption determine the ultimate bioavailability;

a drug having a value of more than 0.90 is considered readily permeable [28]. 0U0and FVV showed

remarkably good permeability, whereas F32 and K11 showed moderate permeability (Table 3), but

3GK and 0JB showed negligible or poor permeability. The human intestine is the primary site for

drug absorption. A previous study suggested that a molecule with >30% absorbency is considered

readily absorbed [27]. Our in-silico absorbance analysis showed that K11 and FVV have very high

absorbance rate 96% and 90% in the human intestine (Table 3), whereas the other compounds exert

moderate >90% absorbance rate. This clearly indicates that all the benzimidazole based ligands have

a high or moderate absorbance rate in the human intestine. All compounds were substrates for P-

glycoprotein, except FVV. Out of six benzimidazole ligands (Table 4).

332

333

334

Table 4. ADMET pharmacokinetics; absorbance and distribution parameters by pKCSM tool and Swiss ADMET server.

| Compoun d name | Water solubilit y (log mol/L) | CaCO ₂ permeabili ty (log Papp in 10 cm/s) | Intestinal absorptio n (human) (% Absorbe d) | Skin Permeabili ty (log Kp) | P- glycoprote in substrate | P- glycoprote in I inhibitor | P- glycoprote in II inhibitor |
|-------------------|--|---|--|-----------------------------------|-------------------------------------|---------------------------------------|--|
| 3GK | -2.892 | -0.179 | 71.399 | -2.735 | Yes | No | No |
| 0U0 | -2.892 | 1.698 | 71.611 | -2.735 | Yes | No | No |
| F32 | -2.912 | 0.072 | 85.508 | -2.735 | Yes | Yes | Yes |
| 0JB | -2.892 | -0.178 | 69.127 | -2.735 | Yes | No | No |
| FVV | -3.04 | 1.718 | 90.072 | -2.69 | No | No | No |
| K11 | -2.892 | 0.251 | 96.374 | -2.735 | Yes | Yes | Yes |

339

340

341

342

343

344

345

346

347

348

349

350

351

352

353

354

336 337

2.4.2. Distribution

The distribution was calculated using the following parameters: human volume of distribution, human fraction unbound in plasma, blood-brain barrier, and central nervous system permeability. In the bloodstream, drugs are generally transported in a free or unbound state or in a partly reversibly bound state. However, irrespective of the transportation state, the steady-state volume of distribution (VDss) remains one of the key pharmacokinetic parameters that must be considered when designing a drug dose range. VDss can be defined as the theoretical volume of a particular drug dose, which vary and give a similar blood plasma concentration. Generally, the greater the VDss value, the more a drug is distributed in tissue rather than plasma. However, for antibiotics and antivirals, more wideranging tissue distribution is desirable [27]. VDss is considered low if the log of the VDss value is lower than -0.15, while a value >0.45 is considered high [27]. Of the six compounds in question, FVV showed the highest distribution value, followed by 0U0 (Table 3). 0JB showed the lowest distribution value among all six compounds. Whereas 3GK, F32, showed moderately low the effectiveness of a drug may vary depending on the limit to which it can bind to blood proteins. The more effective the binding of the drug with blood proteins, the more efficiently the drug compounds can transverse the cellular membrane [27]. Fraction unbound to human plasma ranges between 0.02 to 1.0 [29]. All compounds showed a high fraction unbound value to human plasma (Table 4).

355356

357

358

359

2.4.3. Metabolism

The metabolism of a drug depends upon the molecule being a Cytochrome P450 substrate or inhibitor. 3GK showed moderate inhibition nature where 3GK showed inhibitory activity against

CYP2C19, CYP2C9, CYP3A4 and non-inhibitory effect against CYP1A2 and CYP2D6 of the cytochrome enzymes, whereas 0U0 showed non-inhibitory properties against all enzymes (Table 4). F32and 0JB showed inhibition activity against CYP1A2, CYP2C19, CYP2C9, CYP3A4 and non-inhibitory effects against CYP2D6. FVV showed moderate inhibition nature where FVV showed inhibitory activity against CYP1A2, CYP2C19, CYP2D6cytochrome enzymes and non-inhibitory activity against CYP2C9, CYP3A4. K11also exerts moderate inhibition activity where K11 showed inhibitory activity against CYP1A2, CYP2C19, CYP2C9 and non-inhibitory activity against CYP2D6 and CYP3A4 (Table 4). The results indicate that all benzimidazole ligands will be metabolized by the action of the cytochrome enzymes due to non-inhibitory activities against some cytochrome enzymes (Table 5).

Table 5. ADMET pharmacokinetics; metabolism parameters.

| Compound name | CYP2D6 substrate | CYP3A4 substrate | CYP1A2 inhibitor | CYP2C19 inhibitor | CYP2C9 inhibitor | CYP2D6 inhibitor | CYP3A4 inhibitor |
|---------------|---------------------|------------------|------------------|-------------------|---------------------|---------------------|------------------|
| 3GK | No | No | No | Yes | Yes | No | Yes |
| 0U0 | No | No | No | No | No | No | No |
| F32 | No | Yes | Yes | Yes | Yes | No | Yes |
| ОЈВ | No | No | Yes | Yes | Yes | No | Yes |
| FVV | No | Yes | Yes | Yes | No | Yes | No |
| K11 | No | Yes | Yes | Yes | Yes | No | No |

2.4.4. Excretion

Organic cation transporter 2 (OCT2) belongs to the category of renal uptake transporters, which are known to play important roles during deposition and clearing of drugs from the kidneys [29]. Excretion depends on factors such as total clearance and whether the molecule is a renal OCT2 substrate. Three benzimidazole ligands act as a substrate for Renal OCT2 and can be removed from the body through the renal system. All the selected compounds showed total clearance of less than log (CLtot) 1 mL/min/kg (Table 6).

| Compound | Total Clearance | Renal | Max. tolerated | Oral Rat | Skin | Minnow |
|----------|-----------------|-----------|----------------|----------|---------------|--------|
| name | (log ml/min/kg) | | dose (human) | | Sensitization | |
| | | substrate | (log | Toxicity | | (log |
| | | | mg/kg/day) | (LD50) | | mM) |
| | | | | (mol/kg) | | |
| 3GK | 0.425 | No | 0.469 | 2.457 | No | 2.482 |
| 0U0 | 0.404 | Yes | 0.444 | 2.477 | No | 4.765 |
| F32 | 0.663 | No | 0.471 | 2.459 | No | 2.367 |
| ОЈВ | 0.658 | No | 0.112 | 2.474 | No | 2.051 |
| FVV | 0.826 | Yes | 0.346 | 2.554 | No | 0.754 |
| K11 | 0.484 | Yes | 0.428 | 2.482 | No | -1.64 |

2.3.5. Toxicity

The maximum recommended tolerance dose (MRTD) provides an estimate of the toxic dose in humans. MRTD values less than or equal to $\log 0.477$ ($\log/kg/day$) is considered low [29]. All of six benzimidazole ligands are in the limit of MRTD (Table 4). All six benzimidazole ligands were not skin sensitive (Table 5). A molecule with a high oral rat acute toxicity (LD50) value is less lethal than the lower LD50 value [27]. For a given molecule, the LD50 is the amount that causes the death of 50% of the test animals[27, 30]. All the selected ligands showed high oral rat acute toxicity tolerance (LD50) values (Table 5). The lethal concentration values (LC50) represent the concentration of a molecule necessary to cause 50% of fathead minnow death. For a given molecule, if the $\log LC50 < 0.5 \text{ mM}$ ($\log LC50 < -0.3$), then it is regarded as having high acute toxicity [30, 31]. All six benzimidazole ligands showed a satisfactory score that indicated that they are less toxic than the tolerance limit also (Table 6).

2.4. Lipinsky rule, drug likeliness and bioactivity

Lipinski's rule of five, commonly known as the Pfizer's rule of five or simply the rule of five, is a regulation process to estimate drug-likeness or to identify a chemical compound with a convinced pharmacological or biological activity that has properties that would make it a likely orally active drug in humans. This principle was designed by Christopher A. Lipinski in 1997. The rule expresses molecular properties vital for a drug's pharmacokinetics in the human body, including

- 400 their absorption, distribution, metabolism, and elimination (ADME) components of the Lipinski's
- 401 rule[32].
- 402 Lipinski's rule states:
- 5 or less than 5 hydrogen bond donors (nitrogen or oxygen atoms with one or more hydrogen
- 404 atoms)
- 10 or less than 10 hydrogen bond acceptors (nitrogen or oxygen atoms)
- Molecular weight less than 500 or less.
- Octanol-water partition coefficient log P not greater than 5
- No more than one violation
- The Druglike properties of the selected ligands were evaluated based on Lipinski parameters. Out of
- six benzimidazole ligands two ligands F32 and K11 violates the Lipinski rule as they have slightly
- 411 higher molecular weight. As a rule, it does not predict if a compound is pharmacologically active,
- and the already established antidiabetic and anti-angiogenesis activity in the previous study cannot
- be overlooked [23, 26]. Generally, a molecule showing a negative drug score is not considered a
- promising drug candidate; all six selected molecules show a favorable/positive drug score (Table 7
- and Supplementary Figure S5-S10). All our ligands showed favorable drug likeness therefore we
- 416 proposed six pharmacologically active ligands can be used against VanZ mediated resistance
- 417 treatment.
- Among the six top hits five ligands (3GK, 0U0, F32, 0JB, K11) were found to be highly active
- except FVV towards GPCR ligands. Among the six top hit benzimidazole ligands four (3GK, 0U0,
- 420 0JB, K11) showed high active towards Ion channel modulator and two (F32, FVV) showed moderate
- activity. Four ligands (3GK, 0U0, 0JB, K11) were found to be highly active towards Kinase inhibitor
- and two (F32, FVV) showed moderate activity. Among the six ligands, three (3GK, F32, K11)
- showed moderate activity and the rest three (0U0, 0JB, FVV) no activity score towards nuclear
- receptor ligand. Protease inhibitor: Only one ligand showed highly active property and the rest five
- ligands showed moderate activity towards Protease inhibitor. Except, for one all five ligands were
- found to be highly active towards Enzyme inhibitor. Details in Table 8. In our findings it is clear that
- all six ligands possess high biological activity with their clear categorical ligand behaviors.
- The pharmacological activity depicts the positive impacts of drugs within the living beings. The drug
- 429 is expected to bind with a biological target (usually enzymes, ion channels, and receptors). The
- 430 bioactivity scores of the synthesized complexes can be calculated for several parameters such as
- kinase inhibition, protease inhibition, and enzyme activity inhibition, attaching to G protein-coupled
- 432 receptor (GPCR) ligand and nuclear receptor ligand and ion channel alteration. Molinspiration
- (www.molinspiration.com) was used to calculate these parameters. The bioactivity score is shown in

Table 8. For metal complexes, a bioactivity score more than 0.0 indicates that the complex is active;

if it is between -5.0 and 0.0, then the complex is moderately active, and the bioactivity score is

436 below -5.0 is considered as inactive.

437

438

434

435

Table 7: Drug likeness predicted by Swiss ADME and Mol soft.

| Compound | | Molecular | Number of | Number of | MolLogP | Drug |
|----------|-------------------------|-----------|-----------|-----------|---------|----------|
| name | Lipinski | weight | HBA (<5) | HBD (<10) | (<5) | likeness |
| | (Pfizer)rule | (<500) | | | | (>0) |
| 3GK | Yes | 373.29 | 5 | 3 | 3.46 | 0.3 |
| 0U0 | Yes | 385.15 | 7 | 3 | 1.97 | 0 |
| F32 | Yes | 500.11 | 6 | 3 | 3.98 | 0.98 |
| 0JB | Yes | 305.1 | 5 | 3 | 1.86 | 0.13 |
| FVV | Yes | 281.13 | 1 | 0 | 3.65 | 0.62 |
| K11 | Yes, with one violation | 527.17 | 5 | 3 | 4.32 | 0.28 |

439

Table 8: The bioactivity scores.

| Ligand | GPCR ligand | Ion channel modulator | Kinase inhibitor | Nuclear receptor ligand | Protease inhibitor | Enzyme inhibitor |
|--------|-------------|-----------------------|------------------|-------------------------|--------------------|------------------|
| 3GK | 0.48 | 0.28 | 0.52 | -0.35 | -0.01 | 0.28 |
| 0U0 | 0.35 | 0.48 | 1.25 | -0.76 | -0.02 | 0.33 |
| F32 | 0.02 | -0.09 | -0.08 | -0.3 | -0.03 | 0.49 |
| 0JB | 0.35 | 0.09 | 0.5 | -0.59 | -0.2 | 0.23 |
| FVV | -0.01 | -0.44 | -0.14 | -0.55 | -0.62 | -0.11 |
| K11 | 0.38 | 0.12 | 0.96 | -0.16 | 0.06 | 0.22 |

441

442

2.5MD Simulation analysis

443 *2.5.1 RMSD analysis*

Root Mean Square Deviation (RMSD) measures the quantitative similarity between two superimposed atomic coordinates. RMSD values are presented in Å and calculated by

446

447 RMSD =
$$\sqrt{\frac{1}{n}\sum_{i=1}^{n}d_{i}^{2}}$$

where the averaging is performed over the n pairs of equivalent atoms and d_i is the distance between the two atoms in the ith pair. RMSD can be calculated for any type and subset of atoms; for example, $C\alpha$ atoms of the entire protein, $C\alpha$ atoms of all residues in a specific subset (e.g. the transmembrane helices, binding pocket, or a loop), all heavy atoms of a specific subset of residues, or all heavy atoms in a small-molecule ligands.

To determine VanZ-Benzimidazole ligands conformation stability with drug compounds, 3GK (-10.2 kcal/mol), 0U0 (-9.2 kcal/mol), F32 (-9.1 kcal/mol) 0JB (-9 kcal/mol), FVV (-9 kcal/mol) and k11 (-9 kcal/mol) the backbone root mean square deviation (Cα-RMSD) were computed, as shown in Figure 9. The result shows that the RMSD trajectory of VanZ – 3GK was equilibrated during 0-10 ns and remained steady until 30 ns and a slight drift from 30 ns to 40 ns with an average RMSD value $\sim 6.8 \pm 0.2$ Å at the end of simulation at 40 ns (Figure 6A-black line), which indicates stable structural complexity of the VanZ – 3GK complex. Likewise, the RMSD plot of the VanZ - 0U0 complex equilibrated 0-5 ns and showed a reasonably stable structural complexity during the 40 ns stimulation process. VanZ – 0U0 complex exhibited average RMSD value \sim 6.1 \pm 0.1 Å (Figure 9A-red line). VanZ – F32complexget stabilized around 0-5 ns and exert average~6.8± 0.1 Å RMSD value (Figure 6A-green line).0JB-VanZ complex get stabilized around 0-10 ns and exert average $\sim 5.8 \pm 0.1$ Å RMSD value (Figure 6A-blue line) which represents a highly stable structural complexity. VanZ - FVV complex get stabilized around 0-5 ns and exert average $\sim 5.8 \pm 0.1$ Å RMSD value (Figure 9A-yellow line) which clearly indicated highly structural stability of FVV-VanZ. VanZ - K11 complex get stabilized around 0-10 ns and showed average \sim 6.0 ± 0.1 Å RMSD value (Figure 6A-brown line). Whereas VanZ protein only system showed ~6.0 Å RMSD value and the system equilibrated around 0-10 ns (Figure 6A-grey line). In comparison of protein only system and VanZ – benzimidazole complex system it's clearly visible that VanZ – benzimidazole complex system showed low atomic fluctuations which clearly indicates high structural stability of VanZ – benzimidazole complexes where VanZ – 0JB and VanZ – FVV showed most highly structural stability of protein-ligand structure.

474 2.5.2 RMSF analysis

450

451

452

453

454

455

456

457

458

459

460

461

462

463

464

465

466

467

468

469

470

471

472

473

The RMSF plots of VanZ protein only, VanZ – 3GK, VanZ – 0U0, VanZ – F32, VanZ – 0JB, VanZ – FVV, VanZ – K11, represent that the amino acid residues belonging to termini (N-terminal and C-terminal) and loops have an average atomic fluctuation ~5.0 – ~9.0 Å for VanZ-Benzimidazole complexes, whereas only VanZ protein system showed fluctuations range between ~4.0 – ~5.0 Å (Figure 9B). The RMSF analysis showed mostly the ligand interacting amino acid ranges from 25 to 60, 75 to 115, and 125 to 159 fluctuate the most for better flexibility and during the interaction phase during the 40 ns simulation period. In divergence, the conformational dynamics of stable secondary

structure, α -helices, and β -sheets (interacting protein residues with the ligand compounds) remain

stable during the whole simulation process, providing an indication of the stability of molecular interactions of VanZ with benzimidazole based ligand compounds. The average atomic fluctuations were measured by using RMSF plots, which suggested that all Six Vaz-benzimidazole complexes showed mostly similar fluctuations and flexibility patterns, which clearly indicates that all six benzimidazole based ligands were well accommodated at the binding pocket of VanZ with favorable molecular interactions. RMSF plot suggest VanZ-K11, VanZ-3GK, VanZ-0U0 complexes system showed high flexibility (25-115 amino acid residues) during their interacting phase in comparison of VanZ only system.

2.5.3Rg analysis

- The conformation stability of the VanZ – benzimidazole ligand was evaluated by the radius of gyration (Rg). The Rg parameter is used by computational and structural biologists to describe the structural compactness of proteins. To examine the structural compactness and integrity of VanZ – benzimidazole ligand bound complexes, the radius of gyration (Rg) is calculated for each system [33, 34]. From Figure 9C, it can be observed that the structure of VanZ – 3GK, VanZ – 0JB, VanZ – K11, showed lowest gyration value 17 Å \pm 0.1 which is also similar with VanZ only simulation system and indicates VanZ structural stability in the presence of benzimidazole ligands and maintain as same as VanZ protein system only. Whereas VanZ - 0U0, VanZ - F32, and VanZ - FVV stabilized around an Rg value $18 \text{ Å} - 18.5 \text{ Å} \pm 0.1 \text{ Å}$, which also very close to VanZ protein only system and there was almost no structural drift(Figure 6C). The structural compactness of VanZ – benzimidazole complexes calculated by Rg analyses suggested stable molecular interaction with all six compounds, which are stabilized around $17 - 18.5 \text{ Å} \pm 0.1 \text{ Å}$ (Figure 6C).
- 504 2.5.4 H-Bonds analysis
 - The time evolution plot of hydrogen bond occupancy (H-bonds) between target VanZ and inhibitors was computed. H-bonds are also designated as the "master key of molecular recognition" due their crucial role in ligand binding and enzyme catalysis. Although H-bonds are weaker bonds compared to covalent bonds, their flexibility makes them the most important physical interaction in systems of bio-compounds in aqueous solution. They are critical for maintaining the shape and stability of protein structure. In the case of VanZ 3GKcomplex interaction, initially, 2 H-bonds were detected; however, over time, the number of H-bonds increased, and end of the simulation 3 H-bonds maintained which very close to docking interaction analysis where we also found 2 H-bonds in the docking interaction analysis study. VanZ 0U0 complex showed 2 H-bonds throughout the simulation time as we also found 2 H-bonds during the docking interaction analysis study. VanZ F32 complex H-bond analysis showed 4 H-bonds at end of the simulation which agreed with our

- ocking interaction analysis study. H-bond analysis for VanZ 0JB complex showed 2 H-bond
- 517 interaction existed during the whole simulation process also in docking interaction analysis showed
- 518 the same. No H-bonds were obtained for VanZ FVV complex during the whole simulation process
- also in docking interaction analysis. VanZ K11 complex showed 1 H-bond exist at the end of the
- simulation process, agreed with docking interaction analysis (Figure 9D). Our MD Simulation
- 521 process strongly supports docking and interaction analysis study.
- 522 *2.5.5 SASA analysis*
- 523 Hydrophobic interactions can be considered determinants of protein conformational dynamics.
- Protein conformational dynamics are known to guarantee the structural stability of molecular
- interactions[33, 35]. Computation of the solvent-accessible surface area (SASA) is an important
- parameter when studying changes in structural features of VanZ 3GK, VanZ 0U0, VanZ F32,
- 527 VanZ 0JB, VanZ FVV, VanZ K11 complexes. The proper functioning of protein-ligand
- 528 complexes depend on how well the protein maintains its fold, and how much the protein showed
- 529 interacting surface or pocket for the ligand molecules during the interactions (Figure 9E). shows that
- the complex structure VanZ occupied with the 3GK had an average SASA value of 115.25 nm² \pm 1
- nm². The complex structures VanZ occupied with 0U0, F32, 0JB, FVV, K11 had an average SASA
- value of 96 nm $^2 \pm 1$ nm 2 (Figure 9E). Almost no change in orientation in the protein surface was
- detected for the molecular interaction of VanZ with 0U0, F32, 0JB, FVV, K11. WhetherVanZ
- protein only system showed SASA value 100 nm², except 3GK all ligand occupied VanZ protein
- exert no significant structural changes.
- 536 *2.5.2 Interaction energy analysis*
- The short-range electrostatic (Coul-SR) and van der Waals/hydrophobic (LJ-SR) interaction energies
- between VanZ 3GK, VanZ 0U0, VanZ F32, VanZ 0JB, VanZ FVV, VanZ K11
- 539 complexes explained promising electrostatic as well as hydrophobic interactions. For VanZ 3GK,
- average values of Coul-SR, -50.04 ± 3.4 kJ/mol, and LJ-SR, -172.558 ± 4.0 kJ/mol, were observed.
- For VanZ 0U0, a Coul-SR of -40.32 ± 4.2 kJ/mol and an LJ-SR of -151.51 ± 6.0 kJ/mol were
- observed. VanZ F32 complex exerts a Coul-SR of -34.46 ± 5.3 kJ/mol and an LJ-SR of $-127.31 \pm$
- 4.3 kJ/mol. VanZ 0JB complexes showed a Coul-SR of -34.67 ± 4.4 kJ/mol and an LJ-SR of
- $-134.44 \pm 4.2 \text{ kJ/mol}$. VanZ FVV complexes showed a Coul-SR of $-17.1 \pm 2.1 \text{ kJ/mol}$ and an LJ-
- SR of -128.57 ± 4.2 kJ/mol. VanZ K11 complexes showed a Coul-SR of -22.01 ± 1.3 kJ/mol and
- an LJ-SR of -77.71 ± 2.2 kJ/mol (Figure 9F). This suggested that the role of hydrophobic interaction
- was more important than the electrostatic interactions [36] in stabilizing the complex where 3GK
- showed highest LJ-SR interaction energy and also all the ligands showed gradually LJ-SR

552

553

554

555

556

557

558

559

560

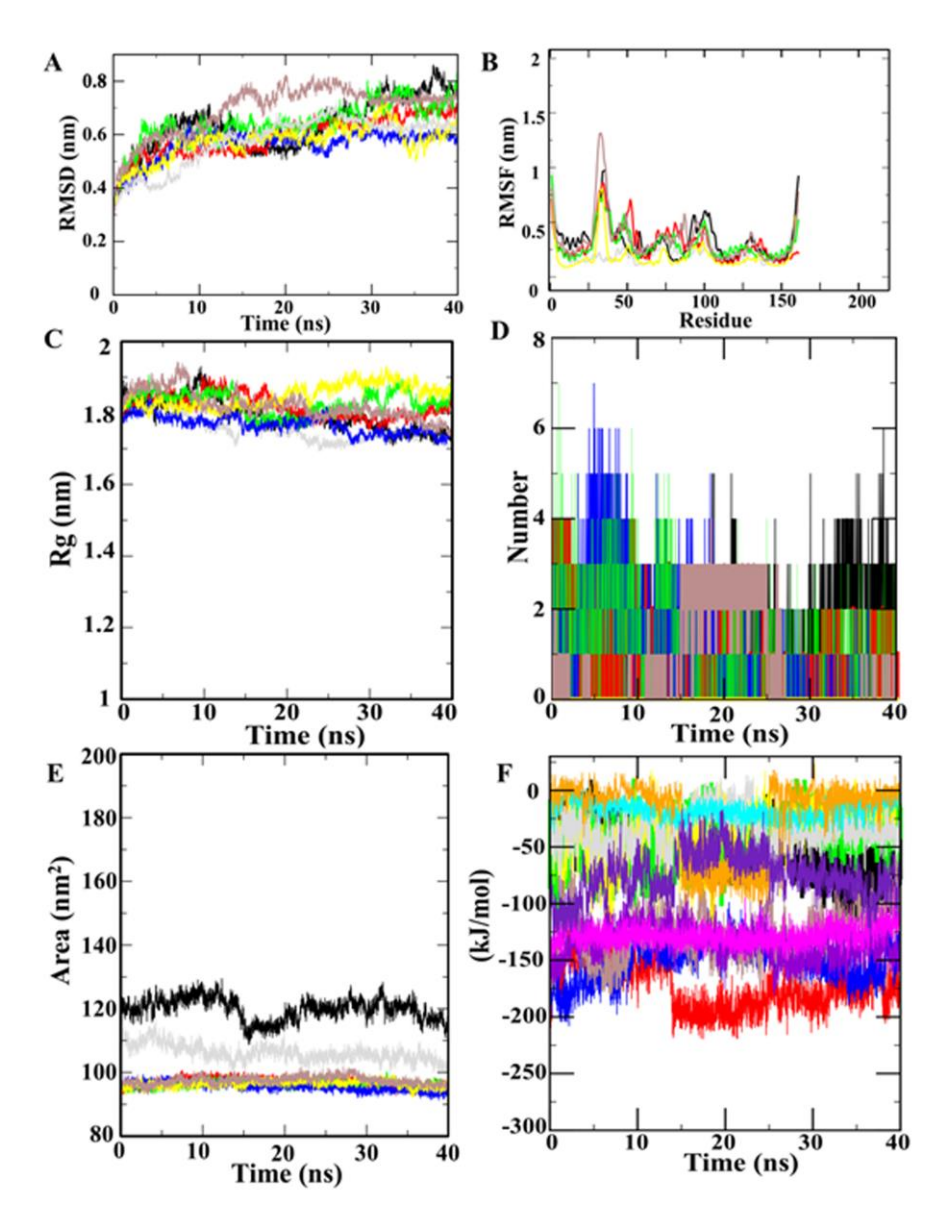


Figure 9. Molecular Dynamic Simulation analysis of best hit benzimidazole ligands against VanZ protein: (A). RMSD plot where the grey line designates VanZ protein only and respective protein ligand complexes are VanZ – 3GK (black), VanZ – 0U0 (red), VanZ – F32 (green), VanZ – 0JB (blue), VanZ – FVV (yellow), VanZ – K11 (brown). (B). RMSF plot where the grey line designates VanZ protein only and respective protein ligand complexes are VanZ – 3GK (black), VanZ – 0U0 (red), VanZ – F32 (green), VanZ – OJB (blue), VanZ – FVV (yellow), VanZ – K11 (brown). (C). Rg plot where the grey line designates VanZ protein only and protein ligand complexes are 3GK- VanZ - 3GK (black), VanZ - 0U0 (red), VanZ - F32 (green), VanZ - 0JB (blue), VanZ - FVV (yellow), VanZ – K11 (brown). (D). H-bond plot where the grey line designate VanZ protein only protein ligand complexes, VanZ – 3GK (black), VanZ – 0U0 (red), VanZ – F32 (green), VanZ – 0JB (blue),

VanZ – FVV (yellow), VanZ – K11 (brown). (E). SASA plot where the grey line designates VanZ protein only protein ligand complexes, VanZ – 3GK (black), VanZ – 0U0 (red), VanZ – F32 (green), VanZ – 0JB (blue), VanZ – FVV (yellow), VanZ – K11 (brown). (F). Interaction energy calculation plot where the grey line designate VanZ protein only and protein ligand complexes, VanZ – 3GK (Coul-SR_black, LJ-SR_red), VanZ – 0JB (Coul-SR_green, LJ-SR_blue), VanZ – F32 (Coul-SR_yellow, LJ-SR_brown), VanZ – 0JB (Coul-SR_grey, LJ-SR_violet), VanZ – FVV (Coul-SR_cyan, LJ-SR_magenta), VanZ – K11 (Coul-SR_orange, LJ-SR_indigo).

569 570

571

572

573

574

575

576

577

578

579

580

581

582

583

584

585

586

587

588

589

590

591

592

593

594

Discussion

Proteins 3D structures help to reveal the function of the molecule. In our previous study we used I-TASSER to predict the de novo structure of the VanZ. The binding pocket was analyzed and 323 benzimidazole based ligands (detail in supplementary) were screened against the VanZ to obtain the best ligands with highest docking scores.

Benzimidazole has its own history in the field of drug development and as protein inhibitors. Benzimidazole derivatives are shown to have pharmacological properties of broad spectrum. They have various activities like antimicrobials, antifungal, antivirals, antiparasitics, anticancers, anticonvulsants, proton pump inhibitors, analgesics, anti-inflammatory agents, antihistaminics, anticoagulants and antihypertensives [37, 38] Benzimidazole derivatives like pantoprazole, lansoprazole, omeprazole and rabeprazole as proton pump inhibitors. Whereas enviradene as antiviral [39] and coumarin-benzimidazole derivatives as a better antibacterial then some commercially available drugs [40]. Benzimidazole was also reported as an inhibitor of mycobacterial DNA gyrase [41]. Further, in our previous study we showed the activity of G3K an benzimidazole based drug against VanZ [5]. Thus, In the present study 323 benzimidazole based ligands were shortlisted based on such reports of biological activities. Six ligands with the best docking scores between -10.2 to -9 kcal/mol were selected (3GK, 0U0, F32, 0JB, FVV, and K11) for further studies. Each ligand has some previously reported biological activity. The 3GK is an investigational drug for the treatment of against beta lactamase bacterial resistance, 0U0 is an investigational molecule against cancerous growth factor, F32 is an investigational drug against diabetes type II, 0JB is an investigational β-Lactamase inhibitory molecule, FVV is an investigational anti-cancer drug and K11 is an investigational angiogenesis drug [25]. And based on the docking results with VanZ, these six have strong protein-ligand interactions. Further depending on the ADMET analysis the ligands are moderately water soluble with good or moderate absorbance rate (permeability – 0U0, FVV, F32. K11 and non-permeable- 3GK and 0JB).

MD simulation showed the interaction of the ligands with the VanZ and its outcomes. The RMSD value was stable for all the ligands after 40ns stimulation without fluctuations showed a stable VanZ-ligands structural complexity and stability for all the size ligands. The RMSD value indicates that the amino acids interacting with the ligands fluctuates the most for better flexibility and interaction. The secondary conformation remained stable during the whole simulation indicating a stable VanZ- size benzimidazole ligands stable interactions. The Rg value of VanZ and VanZ-ligand complex were almost same with nearly no structural drift indicating high compactness of the VanZ protein in presence of the ligands. H bonds and SASA interaction agreed with the docking score and showed no significant changes in the conformation of the dynamics of VanZ protein. Overall, the MD simulations support the docking studying proving the complex formed by the VanZ and 6 different ligands are stable with high structural compactness with very less or no fluctuations.

The toxicity parameters checked showed that all the ligands can be used as a potential candidate for the VanZ inhibitors with the result of toxicity very low. With these we propose that all the six ligands can be a potential inhibitor of the VanZ protein. Further in vitro (such as site-directed mutagenesis studies or quantum mechanics/molecular mechanics simulations) and in vivo studies (such as animal studies, human clinical trials, or studies with cell lines and organoids) will be needed to reveal the actual outcome and to compare the results with the in-silico studies. This study will initiate the follow up studies which can be prevention for the problem in where the *S. aureus* can acquire the VanZ gene which is occasionally transferred from the enterococci. The frequency of which is however very low. The VanZ-bearing mobile genetic element in S. aureus can then interfere with the action of semisynthetic lipoglycopeptide antibiotics.

Materials and methodology

- *3.1. Target and Ligand Preparation*
- 619 1.1. VanZ protein structure prediction and validation
- 620 The VanZ protein sequence (Enterococcus faecium EnGen0191) was obtained from UniProt
- 621 (https://www.uniprot.org/uniprot/Q06242). Thereafter, the I-TASSER webserver
- 622 (http://zhanglab.ccmb.med.umich.edu/I-TASSER/registration.html) was used to obtain the 3D
- 623 structure of VanZ. There are generally four steps involved in the I-TASSER server for structural
- modeling and prediction (https://zhanggroup.org/I-TASSER/about.html) as per our previous work
- 625 [5].
- The 3D SDF structure library of 325 benzimidazole based compounds was downloaded from the
- RCSB (277 ligands), DrugBank 3.0 (38 ligands, https://go.drugbank.com/; accessed on 17 December

- 628 2022), KEGG (8 ligands), and ZINC15 (2 ligands) database (https://go.drugbank.com/; accessed on
- 629 27 January 2023). All compounds were then imported into Open Babel software (Open Babel
- development team, Cambridge, UK) using the PyRx Tool and were exposed to energy minimization.
- The energy minimization was accomplished with the universal force field (UFF) using the conjugate
- gradient algorithm. The minimization was set at an energy difference of less than 0.1 kcal/mol. The
- structures were further converted to the PDBQT format for docking.
- 634 3.2. Protein Pocket Analysis
- 635 The active sites of the receptor were predicted using CASTp
- 636 (http://sts.bioe.uic.edu/castp/index.html?2pk9, accessed on 28 January 2023). The possible ligand-
- binding pockets that were solvent accessible, were ranked based on area and volume.
- 638 3.3. Molecular Docking and Interaction Analysis
- AutoDock Vina 1.1.2 in PyRx 0.8 software (ver.0.8, Scripps Research, La Jolla, CA, USA) was used
- to predict the protein-ligand interactions of the benzimidazole compounds against the VanZ protein.
- The protein and ligand files were loaded to PyRx as macromolecules and ligands, which were then
- converted to PDBQT files for docking. These files were similar to pdb, with an inclusion of partial
- atomic charges (Q) and atom types (T) for each ligand. The binding pocket ranked first was selected
- 644 (predicted from CASTp). Note that the other predicted pockets were relatively small and had lesser
- binding residues. The active sites of the receptor compounds were selected and were enclosed within
- a three-dimensional affinity grid box. The grid box was centered to cover the active site residues,
- with dimensions x = -13.83 Å, y = 12.30 Å, z = 72.67Å. The size of the grid wherein all the binding
- residues fit had the dimensions of x = 18.22 Å, y = 28.11 Å, z = 22.65 Å. This was followed by the
- molecular interaction process initiated via AutoDock Vina from PyRx[5]. The exhaustiveness of
- each of the three proteins was set at eight. Nine poses were predicted for each ligand with the spike
- protein. The binding energies of nine docked conformations of each ligand against the protein were
- recorded using Microsoft Excel (Office Version, Microsoft Corporation, Redmond, Washington,
- 653 USA). Molecular docking was performed using the PyRx 0.8 AutoDock Vina module. The search
- space included the entire 3D structure chain A. Protein-ligand docking was initially visualized and
- analyzed by Chimera 1.15. The follow-up detailed analysis of amino acid and ligand interaction was
- performed with BIOVIA Discovery Studio Visualizer (BIOVIA, San Diego, CA, USA)[42]. The
- 657 compounds with the best binding affinity values, targeting the COVID-19 main protease, were
- selected for further molecular dynamics simulation analysis.
- 659 *3.4. Crosschecking docking and interaction of the top hit ligands*
- Furthermore, top hit molecules were docked through CHARMM force field based swissdock server
- 661 (http://www.swissdock.ch/) for cross checking their binding affinity with VanZ [43]. Interactive

- amino acids and interacting pose was further analyzed by Biovia Discovery Studio Visualizer and
- 663 UCSF Chimera.
- 664 3.5. Absorption, Distribution, Metabolism, Excretion, and Toxicity (ADMET) Analysis
- Pharmacokinetic parameters related to the absorption, distribution, metabolism, excretion, and
- 666 toxicity (ADMET) play a substantial role in the detection of novel drug candidates. To predict
- 667 candidate molecules using in silico methods pkCSM
- 668 (http://biosig.unimelb.edu.au/pkcsm/prediction), webtools were used. Parameters such as AMES
- toxicity, maximum tolerated dose (human), hERG I and hERG II inhibitory effects, oral rat acute
- and chronic toxicities, hepatotoxicity, skin sensitization, and T. pyriformis toxicity and fathead
- 671 minnow toxicity were explored. In addition to these, molecular weight, hydrogen bond acceptor,
- 672 hydrogen bond donor, number of rotatable bonds, topological polar surface area, octanol/water
- partition coefficient, aqueous solubility scale, blood-brain barrier permeability, CYP2D6 inhibitor
- hepatotoxicity, and number of violations of Lipinski's rule of five were also surveyed.
- 675 *3.6. Lipinsky rule, drug lineliness and bioactivity*
- 676 Lipinski's rule of five is helpful in describing molecular properties of drug compounds required for
- estimation of important pharmacokinetic parameters such as absorption, distribution, metabolism,
- and excretion. The rule is helpful in drug design and development. Lipinski's rule of five of the top
- 679 hit six ligands were evaluated by SwissAdme server (http://www.swissadme.ch/).
- Drug likeness of the top hit ligands was evaluated by molsoft server (https://molsoft.com/mprop/).
- Drug score values indicate overall potential of a compound to be a drug candidate. Mol inspiration is
- a web-based tool used to predict the bioactivity score of the synthesized compounds against regular
- human receptors such as GPCRs, ion channels, kinases, nuclear receptors, proteases, and enzymes.
- 684 Bioactivity of the ligands were evaluated by molinspiration server
- 685 (https://www.molinspiration.com/cgi-bin/properties).
- 686 3.7. MD Simulation Studies
- The five best protein-ligand complexes were chosen for MD simulation according to the lowest
- 688 binding energy with the best docked pose. Additional binding interactions were used for molecular
- simulation studies. The simulation was carried out using the GROMACS 2020 package (University
- of Groningen, Groningen, Netherland), utilizing a charmm36 all-atom force field using empirical,
- semi-empirical and quantum mechanical energy functions for molecular systems. The topology and
- 692 parameter files for the input ligand file were generated on the CGenff server
- 693 (http://kenno.org/pro/cgenff/). A TIP3P water model was used to incorporate the solvent, adding
- 694 counter ions to neutralize the system. The energy minimization process involved 50,000 steps for
- each steepest descent, followed by conjugant gradients. PBC condition was defined for x, y, and z

directions, and simulations were performed at a physiological temperature of 300 K. The SHAKE 696 algorithm was applied to constrain all bonding involved, hydrogen, and long-range electrostatic 697 forces treated with PME (particle mesh Ewald). The system was then heated gradually at 300 K, 698 using 100 ps in the canonical ensemble (NVT) MD with 2 fs time step. For the isothermal-isobaric 699 ensemble (NPT) MD, the atoms were relaxed at 300 K and 1 atm using 100 ps with 2 fs time step. 700 701 After equilibrating the system at desired temperature and pressure, the MD run for the system was 702 carried out at 40 ns with time step of 2 fs at 20,000,000 steps. The coordinates and energies were saved at every 10 ps for analysis. 703 704 MD simulation trajectories were analyzed by using a trajectory analysis module integrated into the GROMACS 2020.01 simulation package, qtgrace, VMD, and Chimera software (University of 705 California San Francisco, San Francisco, CA, USA). The trajectory files were first analyzed using 706 GROMCAS tools: gmxrmsd, gmx gyrate, gmxsasa, gmxhbond, gmxcovar, and gmx energy for 707 extracting the graph of root-mean square deviation (RMSD), root-mean square fluctuations 708 709 (RMSFs), radius of gyration (Rg), solvent accessible surface area (SASA), hydrogen bond, principal component, potential energy, kinetic energy, and enthalpy, with python3 free energy surface 710

712

713

711

Author Contributions

calculation and visualization.

- All authors were involved in the data research, manuscript authorship, review and editing of the final article. V.P.S.: conceptualization; methodology; software; visualization; data curation; performance of most of the experiments, including design; protein structure prediction; MD simulation; Pharmacological analysis; and writing the original draft. M.K.S. writing the original draft, review and editing with critical comments: A.M.: writing the original draft, review and editing with the
- 719 critical comments. All authors have read and agreed to the published version of the manuscript.
- 720 **Funding**
- Authors declared no funding acquired for this research.

722723

Institutional Review Board Statement

724 Not applicable.

725 726

Acknowledgments

- 727 We thank the PyRx (https://pyrx.sourceforge.io/) and GROMACS (https://gromacs.bioexcel.eu/)
- team, University of Groningen, Netherlands for use of their freeware dynamic software, cgenff,
- 729 (https://cgenff.umaryland.edu/); webtool servers, RCSB (http://www.rcsb.org/pdb); Drugbank

- 730 (https://go.drugbank.com/); KEGG (https://www.genome.jp/kegg/compound/); ZINC15
- 731 (https://zinc15.docking.org/) CHARMM-GUI (https://www.charmm-gui.org/); SWISSDOCK
- 732 (http://www.swissdock.ch/); MedusaDock (https://dokhlab.med.psu.edu/cpi/#/); pkCSM
- 733 (http://biosig.unimelb.edu.au/pkcsm/prediction); SwissAdme server(http://www.swissadme.ch/);
- 734 Molsoft server (https://molsoft.com/mprop/); Molinspiration server
- 735 (https://www.molinspiration.com/cgi-bin/properties).

737

738

Conflicts of Interest

739 The authors declare no conflict of interest.

740741

Reference

- 742 [1] K.S. O'Brien, P. Emerson, P.J. Hooper, A.L. Reingold, E.G. Dennis, J.D. Keenan, T.M. Lietman, C.E.
- Oldenburg, Antimicrobial resistance following mass azithromycin distribution for trachoma: a systematic review, The Lancet. Infectious diseases 19(1) (2019) e14-e25.
- 745 [2] V.P. Sur, A. Mazumdar, P. Kopel, S. Mukherjee, P. Vítek, H. Michalkova, M. Vaculovičová, A. Moulick, A
- novel ruthenium based coordination compound against pathogenic bacteria, International journal of molecular sciences 21(7) (2020) 2656.
- 748 [3] V.P. Sur, A. Mazumdar, A. Ashrafi, A. Mukherjee, V. Milosavljevic, H. Michalkova, P. Kopel, L. Richtera, A.
- Moulick, A novel biocompatible titanium–gadolinium quantum dot as a bacterial detecting agent with high antibacterial activity, Nanomaterials 10(4) (2020) 778.
- 751 [4] A. Mazumdar, Y. Haddad, V.P. Sur, V. Milosavljevic, S. Bhowmick, H. Michalkova, R. Guran, R. Vesely, A.
- Moulick, Characterization and in vitro analysis of probiotic-derived peptides against multi drug resistance bacterial infections, Frontiers in microbiology 11 (2020) 1963.
- 754 [5] V.P. Sur, A. Mazumdar, V. Vimberg, T. Stefani, L. Androvic, L. Kracikova, R. Laga, Z. Kamenik, K.
- Komrskova, Specific Inhibition of VanZ-Mediated Resistance to Lipoglycopeptide Antibiotics, International Journal of Molecular Sciences 23(1) (2022) 97.
- 757 [6] P. Jelinkova, A. Mazumdar, V.P. Sur, S. Kociova, K. Dolezelikova, A.M.J. Jimenez, Z. Koudelkova, P.K.
- Mishra, K. Smerkova, Z. Heger, M. Vaculovicova, A. Moulick, V. Adam, Nanoparticle-drug conjugates treating bacterial infections, Journal of Controlled Release 307 (2019) 166-185.
- 760 [7] M.K. Annavajhala, A. Gomez-Simmonds, A.-C. Uhlemann, Multidrug-Resistant Enterobacter cloacae 761 Complex Emerging as a Global, Diversifying Threat, Frontiers in Microbiology 10(44) (2019).
- 762 [8] H. Boucher, L.G. Miller, R.R. Razonable, Serious infections caused by methicillin-resistant Staphylococcus 763 aureus, Clin Infect Dis 51 Suppl 2 (2010) S183-97.
- 764 [9] P.S. Loomba, J. Taneja, B. Mishra, Methicillin and Vancomycin Resistant S. aureus in Hospitalized Patients, Journal of global infectious diseases 2(3) (2010) 275-83.
- 766 [10] L.M. Weiner, A.K. Webb, B. Limbago, M.A. Dudeck, J. Patel, A.J. Kallen, J.R. Edwards, D.M. Sievert,
- 767 Antimicrobial-Resistant Pathogens Associated With Healthcare-Associated Infections: Summary of Data
- Reported to the National Healthcare Safety Network at the Centers for Disease Control and Prevention,
- 769 2011-2014, Infection control and hospital epidemiology 37(11) (2016) 1288-1301.
- 770 [11] M. Behnke, S. Hansen, R. Leistner, L.A. Diaz, A. Gropmann, D. Sohr, P. Gastmeier, B. Piening, Nosocomial
- 771 infection and antibiotic use: a second national prevalence study in Germany, Deutsches Arzteblatt
- 772 international 110(38) (2013) 627-33.
- 773 [12] E. Binda, F. Marinelli, G.L. Marcone, Old and New Glycopeptide Antibiotics: Action and Resistance,
- 774 Antibiotics (Basel, Switzerland) 3(4) (2014) 572-94.

- 775 [13] M. Arthur, C. Molinas, T.D. Bugg, G.D. Wright, C.T. Walsh, P. Courvalin, Evidence for in vivo
- incorporation of D-lactate into peptidoglycan precursors of vancomycin-resistant enterococci, Antimicrobial
- 777 agents and chemotherapy 36(4) (1992) 867-9.
- 778 [14] P.E. Reynolds, F. Depardieu, S. Dutka-Malen, M. Arthur, P. Courvalin, Glycopeptide resistance mediated
- by enterococcal transposon Tn1546 requires production of VanX for hydrolysis of D-alanyl-D-alanine,
- 780 Molecular microbiology 13(6) (1994) 1065-70.
- 781 [15] Z. Wu, G.D. Wright, C.T. Walsh, Overexpression, Purification, and Characterization of VanX, a D-, D-
- Dipeptidase which Is Essential for Vancomycin Resistance in Enterococcus faecium BM4147, Biochemistry
- 783 34(8) (1995) 2455-2463.
- 784 [16] M. Arthur, F. Depardieu, P. Reynolds, P. Courvalin, Quantitative analysis of the metabolism of soluble
- 785 cytoplasmic peptidoglycan precursors of glycopeptide-resistant enterococci, Molecular microbiology 21(1)
- 786 (1996) 33-44.
- 787 [17] D. Song, S. Ma, Recent Development of Benzimidazole-Containing Antibacterial Agents, ChemMedChem
- 788 11(7) (2016) 646-659.
- 789 [18] F.A.S. Alasmary, A.M. Snelling, M.E. Zain, A.M. Alafeefy, A.S. Awaad, N. Karodia, Synthesis and
- 790 Evaluation of Selected Benzimidazole Derivatives as Potential Antimicrobial Agents, Molecules 20(8) (2015)
- 791 15206-15223.
- 792 [19] R.S. Keri, A. Hiremathad, S. Budagumpi, B.M. Nagaraja, Comprehensive Review in Current
- 793 Developments of Benzimidazole-Based Medicinal Chemistry, Chemical biology & drug design 86(1) (2015)
- 794 19-65.
- 795 [20] V. Vimberg, L. Zieglerová, K. Buriánková, P. Branny, G. Balíková Novotná, VanZ Reduces the Binding of
- 796 Lipoglycopeptide Antibiotics to Staphylococcus aureus and Streptococcus pneumoniae Cells, Frontiers in
- 797 Microbiology 11 (2020).
- 798 [21] D.A. Nichols, J.C. Hargis, R. Sanishvili, P. Jaishankar, K. Defrees, E.W. Smith, K.K. Wang, F. Prati, A.R.
- 799 Renslo, H.L. Woodcock, Y. Chen, Ligand-Induced Proton Transfer and Low-Barrier Hydrogen Bond Revealed
- by X-ray Crystallography, Journal of the American Chemical Society 137(25) (2015) 8086-8095.
- 801 [22] E.A. Peterson, A.A. Boezio, P.S. Andrews, C.M. Boezio, T.L. Bush, A.C. Cheng, D. Choquette, J.R. Coats,
- A.E. Colletti, K.W. Copeland, M. DuPont, R. Graceffa, B. Grubinska, J.L. Kim, R.T. Lewis, J. Liu, E.L. Mullady,
- 803 M.H. Potashman, K. Romero, P.L. Shaffer, M.K. Stanton, J.C. Stellwagen, Y. Teffera, S. Yi, T. Cai, D.S. La,
- Discovery and optimization of potent and selective imidazopyridine and imidazopyridazine mTOR inhibitors,
- 805 Bioorganic & Medicinal Chemistry Letters 22(15) (2012) 4967-4974.
- 806 [23] P.J. Ala, L. Gonneville, M. Hillman, M. Becker-Pasha, E.W. Yue, B. Douty, B. Wayland, P. Polam, M.L.
- 807 Crawley, E. McLaughlin, R.B. Sparks, B. Glass, A. Takvorian, A.P. Combs, T.C. Burn, G.F. Hollis, R. Wynn,
- 808 Structural Insights into the Design of Nonpeptidic Isothiazolidinone-containing Inhibitors of Protein-tyrosine
- 809 Phosphatase 1B *, Journal of Biological Chemistry 281(49) (2006) 38013-38021.
- 810 [24] D.A. Nichols, P. Jaishankar, W. Larson, E. Smith, G. Liu, R. Beyrouthy, R. Bonnet, A.R. Renslo, Y. Chen,
- 811 Structure-Based Design of Potent and Ligand-Efficient Inhibitors of CTX-M Class A β-Lactamase, Journal of
- 812 medicinal chemistry 55(5) (2012) 2163-2172.
- 813 [25] T.R. Hodges, J.R. Abbott, A.J. Little, D. Sarkar, J.M. Salovich, J.E. Howes, D.T. Akan, J. Sai, A.L. Arnold, C.
- 814 Browning, M.C. Burns, T. Sobolik, Q. Sun, Y. Beesetty, J.A. Coker, D. Scharn, H. Stadtmueller, O.W.
- Rossanese, J. Phan, A.G. Waterson, D.B. McConnell, S.W. Fesik, Discovery and Structure-Based Optimization
- 816 of Benzimidazole-Derived Activators of SOS1-Mediated Nucleotide Exchange on RAS, Journal of medicinal
- 817 chemistry 61(19) (2018) 8875-8894.
- 818 [26] V.J. Cee, A.C. Cheng, K. Romero, S. Bellon, C. Mohr, D.A. Whittington, A. Bak, J. Bready, S. Caenepeel, A.
- 819 Coxon, H.L. Deak, J. Fretland, Y. Gu, B.L. Hodous, X. Huang, J.L. Kim, J. Lin, A.M. Long, H. Nguyen, P.R. Olivieri,
- 820 V.F. Patel, L. Wang, Y. Zhou, P. Hughes, S. Geuns-Meyer, Pyridyl-pyrimidine benzimidazole derivatives as
- 821 potent, selective, and orally bioavailable inhibitors of Tie-2 kinase, Bioorganic & Medicinal Chemistry Letters
- 822 19(2) (2009) 424-427.
- 823 [27] S. Saha, R. Nandi, P. Vishwakarma, A. Prakash, D. Kumar, Discovering Potential RNA Dependent RNA
- 824 Polymerase Inhibitors as Prospective Drugs Against COVID-19: An in silico Approach, Frontiers in
- 825 pharmacology 12 (2021) 267.

- 826 [28] A. Chandra, M. Chaudhary, I. Qamar, N. Singh, V. Nain, In silico identification and validation of natural
- antiviral compounds as potential inhibitors of SARS-CoV-2 methyltransferase, Journal of Biomolecular
- 828 Structure and Dynamics (2021) 1-11.
- 829 [29] S. Tamura, G.-M. Yang, N. Yasueda, Y. Matsuura, Y. Komoda, N. Murakami, Tellimagrandin I, HCV
- 830 invasion inhibitor from Rosae rugosae Flos, Bioorganic & medicinal chemistry letters 20(5) (2010) 1598-
- 831 1600.
- 832 [30] D. Bhowmik, R. Nandi, R. Jagadeesan, N. Kumar, A. Prakash, D. Kumar, Identification of potential
- inhibitors against SARS-CoV-2 by targeting proteins responsible for envelope formation and virion assembly
- using docking based virtual screening, and pharmacokinetics approaches, Infection, Genetics and Evolution
- 835 84 (2020) 104451.
- 836 [31] M. Sinha, R. Jagadeesan, N. Kumar, S. Saha, G. Kothandan, D. Kumar, In-silico studies on Myo inositol-1-
- 837 phosphate synthase of Leishmania donovani in search of anti-leishmaniasis, Journal of Biomolecular
- 838 Structure and Dynamics (2020) 1-14.
- 839 [32] C.A. Lipinski, F. Lombardo, B.W. Dominy, P.J. Feeney, Experimental and computational approaches to
- 840 estimate solubility and permeability in drug discovery and development settings, Advanced drug delivery
- 841 reviews 46(1-3) (2001) 3-26.
- 842 [33] A. Prakash, V. Kumar, N.K. Meena, A.M. Lynn, Elucidation of the structural stability and dynamics of
- heterogeneous intermediate ensembles in unfolding pathway of the N-terminal domain of TDP-43, RSC
- 844 advances 8(35) (2018) 19835-19845.
- 845 [34] M. Nygaard, B.B. Kragelund, E. Papaleo, K. Lindorff-Larsen, An efficient method for estimating the
- hydrodynamic radius of disordered protein conformations, Biophysical journal 113(3) (2017) 550-557.
- 847 [35] P. Banerjee, B. Bagchi, Dynamical control by water at a molecular level in protein dimer association and
- dissociation, Proceedings of the National Academy of Sciences 117(5) (2020) 2302-2308.
- [36] D.M. Teli, M.B. Shah, M.T. Chhabria, In silico Screening of Natural Compounds as Potential Inhibitors of
- SARS-CoV-2 Main Protease and Spike RBD: Targets for COVID-19, Frontiers in molecular biosciences 7 (2020) 599079.
- 852 [37] F. Fei, Z. Zhou, New substituted benzimidazole derivatives: a patent review (2010 2012), Expert Opin
- 853 Ther Pat 23(9) (2013) 1157-79.
- 854 [38] S.R. Brishty, M.J. Hossain, M.U. Khandaker, M.R.I. Faruque, H. Osman, S.M.A. Rahman, A
- 855 Comprehensive Account on Recent Progress in Pharmacological Activities of Benzimidazole Derivatives,
- 856 Frontiers in Pharmacology 12 (2021).
- 857 [39] P.K. Singh, O. Silakari, Chapter 2 Benzimidazole: Journey From Single Targeting to Multitargeting
- Molecule, in: O. Silakari (Ed.), Key Heterocycle Cores for Designing Multitargeting Molecules, Elsevier2018,
- 859 pp. 31-52.
- 860 [40] L.R. Singh, S.R. Avula, S. Raj, A. Srivastava, G.R. Palnati, C.K.M. Tripathi, M. Pasupuleti, K.V. Sashidhara,
- 861 Coumarin-benzimidazole hybrids as a potent antimicrobial agent: synthesis and biological elevation, The
- 862 Journal of Antibiotics 70(9) (2017) 954-961.
- 863 [41] P.S. Hameed, A. Raichurkar, P. Madhavapeddi, S. Menasinakai, S. Sharma, P. Kaur, R. Nandishaiah, V.
- 864 Panduga, J. Reddy, V.K. Sambandamurthy, D. Sriram, Benzimidazoles: novel mycobacterial gyrase inhibitors
- from scaffold morphing, ACS Med Chem Lett 5(7) (2014) 820-5.
- 866 [42] V.P. Sur, M.K. Sen, K. Komrskova, In Silico Identification and Validation of Organic Triazole Based Ligands
- as Potential Inhibitory Drug Compounds of SARS-CoV-2 Main Protease, Molecules 26(20) (2021) 6199.
- 868 [43] A. Grosdidier, V. Zoete, O. Michielin, SwissDock, a protein-small molecule docking web service based on
- 869 EADock DSS, Nucleic acids research 39(Web Server issue) (2011) W270-7.